A city against the current: A reconstruction of Holocene sea-level changes and the evolution of coastal landscapes in ancient Abdera (Thrace, Gr.)

Alfredo Mayoral [a,b,*], Ana Ejarque [c], Arnau Garcia-Molsosa [a], Mercourios Georgiadis [a], Giannis Apostolou [a], Vincent Gaertner [d], Constantina Kallintzi [e], Eurydice Kefalidou [f], Hèctor Orengo [a,g]

[a] ICAC - Catalan Institute of Classical Archaeology, Landscape Archaeology Research Group (GIAP), Plaça Rovellat s/n, 43003 Tarragona, Spain
[b] Université Clermont Auvergne, CNRS, GEOLAB, F-63000 Clermont-Ferrand, France
[c] ISEM, Univ Montpellier, CNRS, IRD, France
[d] CNRS, UMR 5600, EVS-IRG & University of Lyon, France
[e] Emeritus Ephor of Antiquities, A. Symeonidou 5, Komotini, GR 67132, Greece
[f] National and Kapodistrian University of Athens, School of Philosophy, Department of History and Archaeology, Athens 157 84, Greece
[g] Catalan Institution for Research and Advanced Studies (ICREA), Passeig Lluís Companys, 23, 08010 Barcelona, Spain

ARTICLE INFO

ABSTRACT

This paper presents an integrated Geoarchaeological approach to Holocene landscape change and socio-environmental interaction around ancient Abdera, a Greek colony in Aegean Thrace. A combination of remote sensing, geomorphological mapping, sedimentary coring, and radiocarbon dating was used to build the first detailed Holocene sea-level curve in the Northern Aegean, and to reconstruct the palaeogeographic evolution around Abdera from the Neolithic onwards. The discussion of these results, alongside the available archaeo-historical data, sheds new light on the role of historical and environmental factors in the rise and eventual decline of Abdera, thereby challenging previous narratives. This study is the first to detect evidence of the Neolithic landscapes in this coastal area being submerged by marine transgression c. 5000 cal. BC. A lagoonal landscape developed from the Neolithic until Greek colonists settled in the area c. 654 BC. The results presented here suggest that the relocation of the city in the 4th century BC was not caused by the silting up of the bay but was due to historical events. The coastal progradation only became significant after 300 cal. BC and accelerated in the following centuries. Based on the data acquired, it is hypothesized that this was due to anthropogenic forcing of the sedimentary systems both at local and regional levels, caused by the development of the productive activities of the colony. The evidence presented here demonstrates that while Abdera retained good access to the sea, its decline in the 4th c. AD was certainly due to the gradual shift of the economic axis inland. By 400 cal. AD the coastline was very close to its current position. The results of this study also add to the catalogue of known tsunamis in the Northern Aegean, by providing new evidence of a tsunami on this section of the Thracian coast in 544 AD.

1. Introduction

Current Mediterranean landscapes are the result of a complex interplay between socio-cultural practices and environmental dynamics that have taken place since the Neolithic. This process of socio-environmental interaction has shaped specific cultural landscapes over millennia, which in themselves constitute a significant form of heritage (Blondel, 2006). This is particularly evident in Mediterranean coastal areas: these highly diverse natural systems, which are the loci of very active eco- and geomorphological dynamics, have acted as interfaces where interaction between changing climate, environments, and societies has been particularly intense and intricate since Prehistory (e.g., Cañellas-Boltà et al., 2018, Florenzano et al., 2022). However, these Mediterranean coastal landscapes and the natural and cultural heritage they represent are currently endangered due to anthropogenic factors, such as accelerated climate change, rapid sea-level rise, or extensive

---

* Corresponding author.
E-mail address: amayoral@icac.cat (A. Mayoral).

urbanization associated with the destruction of habitats and traditional landscapes (Cramer et al., 2018; Malek et al., 2018). Understanding how past societies interacted with their environments at different geographical and temporal levels presents a crucial challenge not only to the ability to unravel the genesis of Mediterranean coastal landscapes, but also to how we understand their present-day dynamics, promote and protect their fragile heritage, and ensure their sustainable management in the changing world of the Anthropocene (Dearing et al., 2015; Steffen et al., 2015; Waters et al., 2016; Zalasiewicz et al., 2017).

The geoarchaeological approach (*sensu* Butzer, 1982, 2005) is definitely one of the most powerful tools available to allow the fulfilment of these goals as it can efficiently track key natural and anthropogenic processes shaping coastal Mediterranean landscapes (Morhange et al., 2011). Indeed, geoarchaeological studies can provide valuable data on how ancient societies and settlements adapted to and interacted with rising sea-levels in the Holocene (e.g. Brisset et al., 2018), dynamic equilibrium between shore erosion and sedimentation (Stock et al., 2016; Giaime et al., 2019; Amato et al., 2021), palaeogeographic changes (Kraft et al., 2007; Vött et al., 2007; Brückner et al., 2013; Salomon et al., 2018; Giaime et al., 2022), the hydro-ecological state of wetlands (e.g. Ejarque et al., 2016), or the impacts of extreme events (e.g. Lespez et al., 2021). Among the many case studies where these topics can be investigated, *ex novo* urban settlements in previously unoccupied coastal areas provide an excellent opportunity to detect land-use impacts against the pre-settlement background. Such contexts also allow a more direct identification and discussion of the mechanisms behind socio-environmental interaction and landscape change.

Within this framework, the foundation of Greek colonies during the Archaic Period is of exceptional interest. These sites were often founded in selected coastal locations, which were relatively marginal and uninhabited by native populations. Furthermore, they were often surrounded by wetlands that are likely to provide good sedimentary records for palaeoenvironmental studies. Therefore, they offer an opportunity for an accelerated and intense shift in socio-environmental interaction to be observed, due to sudden urbanization and demographic increase in a restricted area, accompanied by the implementation of particular settlement and land-use patterns that were focused on specific local resources to satisfy the precise productive needs of the city (Kaniewski et al., 2013; Marriner et al., 2014). These changes impacted and transformed previous environments, and ultimately led to the construction of new landscapes that have lasted in great part until the present day.

The general aim of this work is to assess the role of environmental factors and human impact on long-term socio-environmental interaction and landscape evolution around the ancient city of Abdera, an Ionian colony in Aegean Thrace where geoarchaeological and palaeoenvironmental data are scarce. The specific objectives were to reconstruct Holocene Relative-Sea-Level changes and the palaeogeographic evolution of the area, to assess the incidence of key coastal processes, such as coastal progradation or marine extreme phenomena, and to discuss the interaction of these natural processes with human societies, particularly the Greek colony of Abdera.

In order to reach these objectives, a broad, integrated geoarchaeological approach was employed to explore Holocene stratigraphy and sedimentary archives around the city, including remote sensing, geomorphological mapping, drilling of sedimentary cores, litho-stratigraphic, and pedo-sedimentary descriptions, alongside the reconstruction of sedimentary environments and the Relative Sea-Level during the Holocene. The results were interpreted within a robust radiocarbon-based chrono-stratigraphic framework, integrated, and then discussed together with archaeological and historical data from excavations, recent surveys, and written sources, thereby providing a comprehensive overview of socio-environmental interaction and allowing us to discuss causality in terms of landscape change in the area from the Neolithic to Late Roman period.

2. Regional setting

2.1. Geographical settings

The study is focused on the area surrounding the ancient colony of Abdera, on the Thracian coast of the northern Aegean (Fig. 1). In this sector of Thrace, the steep Rhodope range looms over a relatively narrow coastal plain with three main physical and morphological units. In the SW, the large fan-shaped Nestos delta is covered by alluvial deposits which have been accumulating since the Plio-Pleistocene (Stournaras, 1984). The central area of the plain is occupied by the Abdera horst, a block that raised during the Alpine orogeny. It has a diverse lithology, which is mainly gneissic in the area of the Greek colony (IGME, 1980). The Vistonis plain is a large Pleistocene to Holocene alluvial surface located between the foothills of the Rhodope mountains and the Vistonis lake. Littoral areas are shaped by waves and currents, with sandy beaches, dunes, marshlands, and lagoons, with a microtidal regime (IGME, 1980; Stournaras, 1984; Xeidakis et al., 2010). In this portion of the coast NE winds and coastal currents prevail, although winds of a reverse NW direction occasionally occur (Kourafalou & Barbopoulos, 2003; Xeidakis et al., 2010; Kokkos et al., 2021).

Cape Bouloustra, where the ancient colony of Abdera was founded, is the only rocky promontory (36 m a.s.l.) on this sandy coast and it is connected to the mainland by a narrow "neck" on its north side (Fig. 2). The small gneissic massif lies at the headwaters of several short valleys with ephemeral streams running West and East from the central ridge and is almost surrounded by coastal wetlands and marshes (<2 m a.s.l.). These are particularly developed on the W side of the colony but are in the main part drained. The area is largely cultivated, with small patches of trees and shrubs growing in drier sandy emerged areas, and fresh and salt marshes developing in the wet lowlands. The soil cover includes long-term evolution reddish soils in raised areas, and much younger, incipient soils which developed in the alluvial and coastal deposits of the lowlands.

2.2. Archaeological and geomorphological background

Data concerning human settlements and societies before the Iron Age in the region (see Table 1 for the chronological framework in NE Greece) are rather scarce. One of the few significant prehistoric sites recorded in this coastal area is a partly underwater shell mound adjacent to the Lafrouda lagoon, a few kms NE of the study area, and dated c. 5500–5200 cal. BC. The few documented Iron Age Thracian sites are mostly located inland in the foothills of the Rhodope mountains (Kallintzi, 2011; Kallintzi et al., 2021).

The main historical event in the area was foundation of the Greek colony of Abdera around 654 BC by Ionian colonists from Klazomenai. It was re-settled later by Teians in 545 BC (Moustaka et al., 2004; Kallintzi, 2011) and quickly became a wealthy and prosperous city. From the 5th to the 2nd centuries BC, Abdera was initially under Persian control (512-475 BC), and then became a member of the Delian league. Finally, it came under the rule of the Macedonian and Diadochi kingdoms until 168 BC when Rome imposed its dominion over Thrace. The city gradually went into decline in the subsequent centuries, and after the 4th c. AD only a reduced byzantine settlement (the Polystylon) with a small harbour remained in occupation until the 14th c. AD (Kallintzi et al., 2001; Kallintzi, 2018).

The site includes two adjacent walled enclosures or *enceintes*: the northern one, which is largely unexcavated, corresponds to the Archaic and Classical city and was occupied from the 7th to at least the 4th or the early 3rd century BC (see Georgiadis et al., 2022). In the middle of the 4th c. BC a new city was built within a second *enceinte* that lay slightly to the south, an area which has been the focus of recent excavations (Fig. 3). This major urban shift has traditionally been interpreted as the relocation of the city during Hellenistic and Roman periods. Both *enceintes* are surrounded by hundreds of funerary *tumuli* dating from the
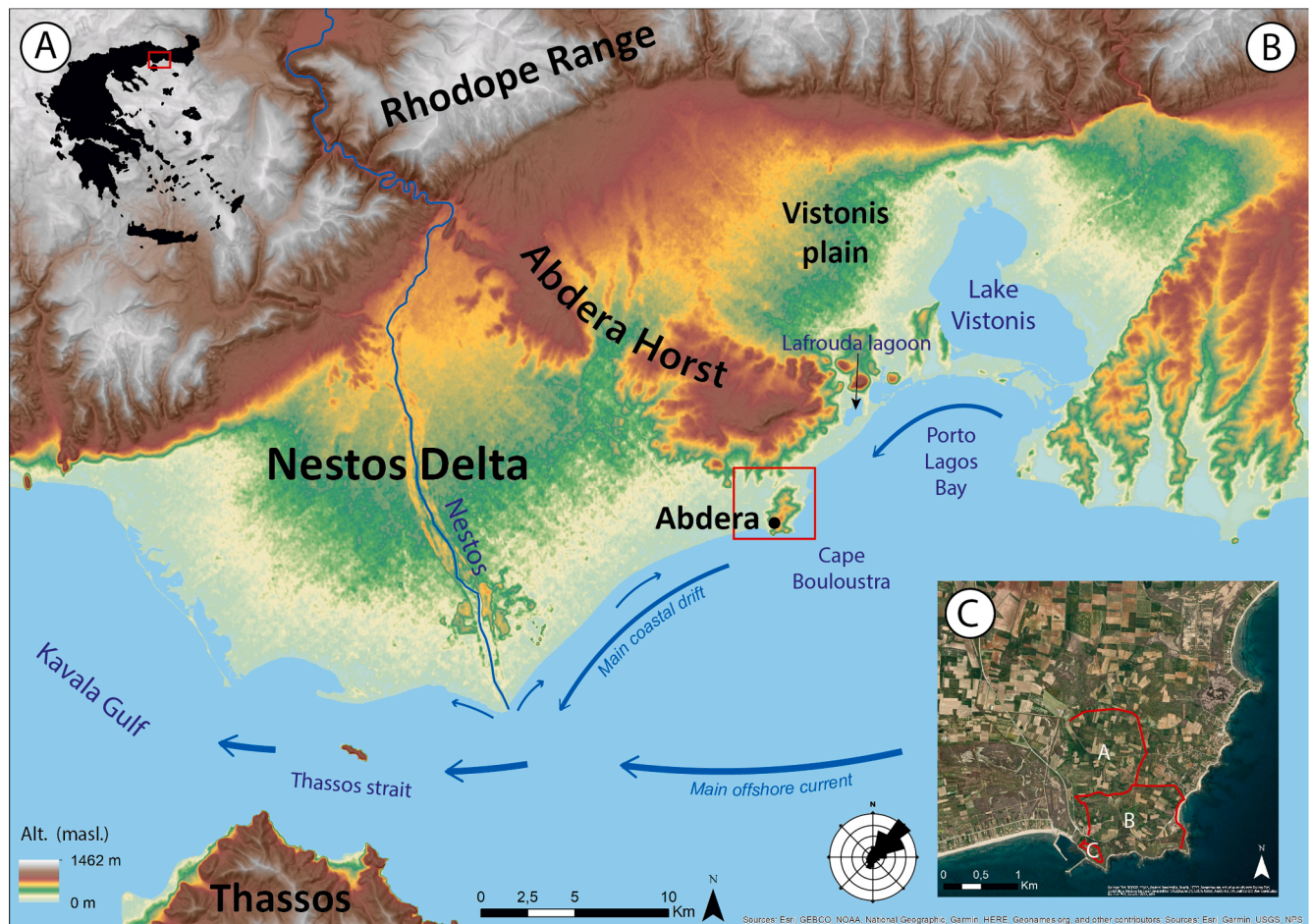
Fig. 1. The location and physical context of the study area. A) The location in NE Greece. B) Relief map of the Thracian coastal plain between the Kavala Gulf and Lake Vistonis (based on ALOS30 DEM, see methods). The red frame represents the study area. The currents are adapted from Kourafalou & Barbopoulos, 2003 and Xeidakis et al., 2010; the winds from Kokkos et al., 2021. C) The study area: the location on Cape Bouloustra of the ancient city of Abdera (enceintes A – the Archaic to Classical city- and B -the Hellenistic to Roman city-), and the Byzantine Polystylon (enceinte C), see Fig. 3 for details. Background: Esri World Imagery. (For interpretation of the references to colour in this figure legend, the reader is referred to the web version of this article.)

6th to the 3rd centuries BC (Moustaka et al., 2004). Based on the location of several of the ancient harbour facilities up to a distance of 2 km inland (Fig. 3, see Kallintzi, 2011), a preliminary geomorphological study carried in the 80s found that a deep embayment may have existed at the time of the Klazomenian foundation on the western side of the Cape. This study proposed that this embayment may have gradually silted up over later periods probably due to a massive supply of sediments from the Nestos River (Syrides & Psilovikos, 2004). However, the limited detail and a lack of chronological precision marks this palaeogeographic reconstruction which has hampered its correlation with archaeological data and thus prevented any fine interpretations. To overcome these limitations, geomorphological and geoarchaeological research has been carried out around Abdera since 2020 as part of the APAX, TransLands, and TransMed projects, which has yielded considerable new data that are presented in this paper.

3. Materials and methods

3.1. Remote Sensing, cartographic data and geomorphological mapping

Historical aerial imagery was obtained from different photographic flights provided by the Hellenic Military Geographical Service (1938, 1945, 1960, 1978, 1989, 2002), and more recently imagery was gathered from Google Earth, Microsoft Zoom Earth, and Esri World Imagery. Satellite imagery from Sentinel 2 (2015 onwards) was processed to

obtain the Seasonal Multi-Temporal Vegetation Indices (SMTVI, see Fig. 5), which have provided useful composite imagery for the detection of geomorphological features (Orengo & Petrie, 2017).

Several Digital Elevation Models (DEMs) with different resolutions and coverage ranging from macroscale to detail scale were combined to cover all the study area. ALOS30 and EUDEM25, two large-scale DEMs with global coverage and a similar resolution (30 and 25 m/pixel respectively), were used as background topographic data. Aerial imagery obtained in 1978 (see above) was used to produce, through digital photogrammetry, a DEM with an intermediate resolution of 3 m covering the whole study area. Finally, several small areas were covered by drone flights using a DJI Phantom 4 Pro, and the resulting aerial imagery was used to produce high-resolution photogrammetric DEMs (of a cell size of 1 m to 15 cm). From all of these DEMs a series of contour lines and basic derived models were produced such as slope or hillshade models, in order to improve relief visualization (Mayoral et al., 2017; Orengo and Petrie, 2018). Additionally, a series of maps were consulted including 1:50.000 soviet topographic maps dating from 1976, 1980, and 1981, which were compiled and georeferenced by the University of Plovdiv (BGTopoVJ), the topographic maps available online from the Hellenic Military Geographical Service (GeoIndex viewer), and a geological 1:50.000 map by the IGME (sheet n° 48 Avdhira-Mesi, 1980).

All these remotely sensed and cartographic sources were compiled and entered into ArcGIS 10.4 (ArcMap and ArcScene) and then exploited for geomorphological mapping and general cartographic purposes.
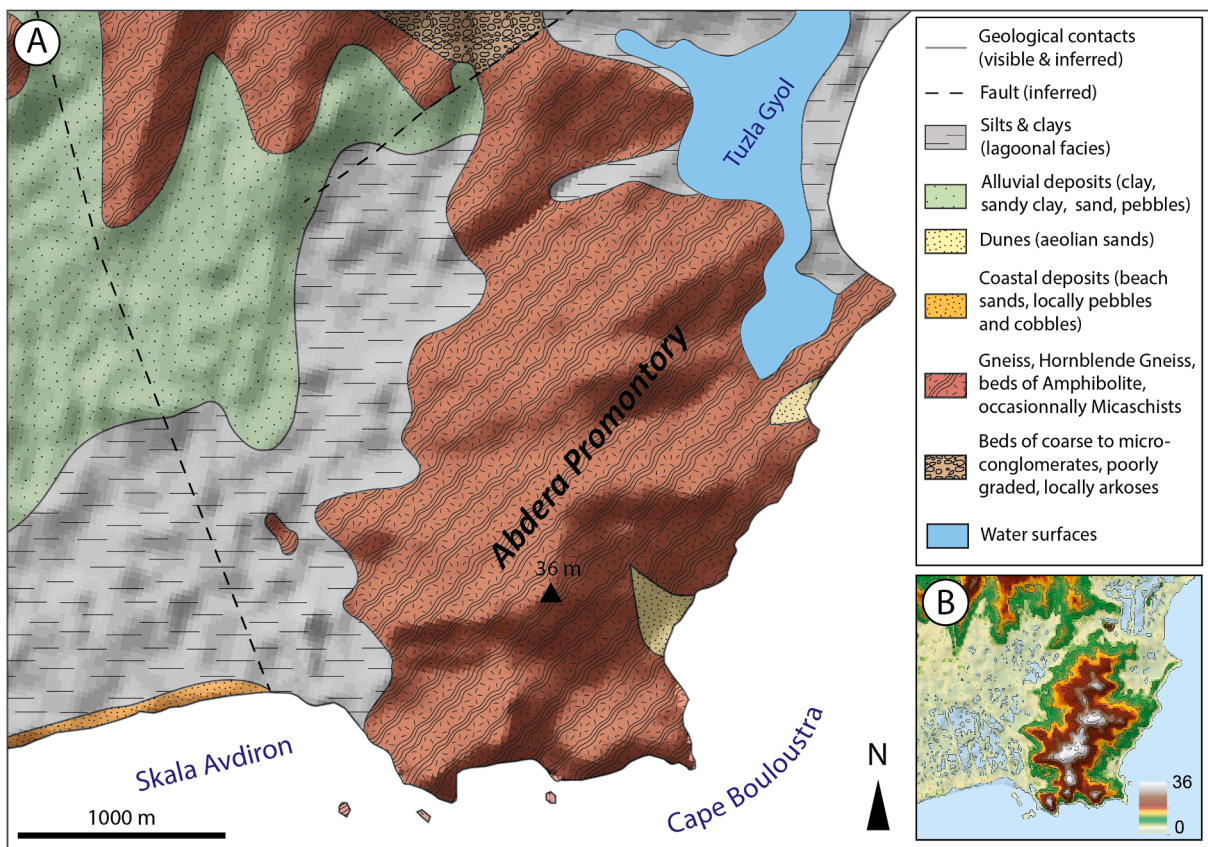
Fig. 2. A) Shaded geological sketch of the study area, after the IGME 1:50.000 sheet n°48 Avdhira-Mesi (IGME, 1980). B) Hipsometric map of the study area based on the ALOS30 Digital Elevation Model.

Table 1
Chronological framework in NE Greece (after Kallintzi et al., 2001; Glais, 2017).

Archaeological and Historical periods		Years BC/AD
NEOLITHIC	Early Neolithic	6500–5700 BC
(6500–3150 BC)	Middle Neolithic	5700–5400 BC
	Late Neolithic I	5400–4850 BC
	Late Neolithic II	4850–4250 BC
	Late Neolithic III / Final Neolithic	4250–3150 BC
BRONZE AGE	Early Bronze Age I	3150–2800 BC
(3150–1000 BC)	Early Bronze Age II	2800–2150 BC
	Middle Bronze Age	2150–1600 BC
	Late Bronze Age	1600–1000 BC
IRON AGE (1000–800 BC)	Early Iron Age	1000–800 BC
ANTIQUITY	Archaic period	800–480 BC
(800 BC-324 AD)	Classical period	480–323 BC
	Hellenistic period	323–31 BC
	Roman period	31 BC-324 AD
BYZANTINE		324–1453 AD
OTTOMAN		1453–1920 AD
CONTEMPORARY		1920 AD onwards

During the fieldwork campaigns, targeted survey focused on specific areas of the landscape was performed in order to characterize landforms and superficial deposits in greater detail, but also to cross-check, complete, and refine the remotely sensed information before the final mapping stage.

3.2. Sedimentary Coring, litho-stratigraphic description and facies interpretation

During the two field seasons of July and September/October 2020 a total of 140 m of sedimentary records were drilled that were distributed across 19 coring points (individual cores with lengths from 140 to 823 cm), following five coring transects on both sides of the colony (see Fig. 6). An array of coring techniques and instruments were used, including a hand auger, a Russian corer, and an Atlas Copco Cobra TT percussion corer. The latter was used with both open samplers (gouge) of different diameters and with a PVC liner (diameter 5 cm), in order to recover undisturbed sedimentary cores. The points of coring were recorded as XYZ coordinates with a centimetric DGPS with an RTK station adapted to the Greek Grid. All altitudes are given in the Greek datum.

The drilling samples performed with a hand auger and with gouges (percussion corer) were photographed, described, and sampled for ^{14}C dating directly in the field. Russian coring and cobra coring samples were taken with a PVC liner and were treated in the laboratory: after the opening and cleaning of the tubes, all the half-sections of the cores were photographed at high resolution and sampled for radiocarbon dating. Litho-stratigraphic descriptions were performed including all their relevant pedo-sedimentary features. Depths were carefully measured and sediment compaction (which is always < 10%) was corrected when necessary. When required, multi-core composite sequences were built using several drilling samples available from the same point. Sediment samples were also occasionally sieved and observed under the binocular microscope, allowing qualitative characterization of mineralogy and organic matter among other features. The most frequent and typical malacological species visible in the surface of the cores were included in the macroscopic description and identified at genus level: *Cerastoderma* sp., *Cerithium* sp., *Tritia* sp., *Loripes* sp., *Abra* sp., *Bittium/Potamides* sp. and *Trochidae*. Although they were not quantified, they were used as an additional qualitative indicator of the sedimentary environment, which, in most cases, was quiet water conditions matching low-energy coastal lagoons with variable connections with the sea (Koutsoubas et al., 2000;
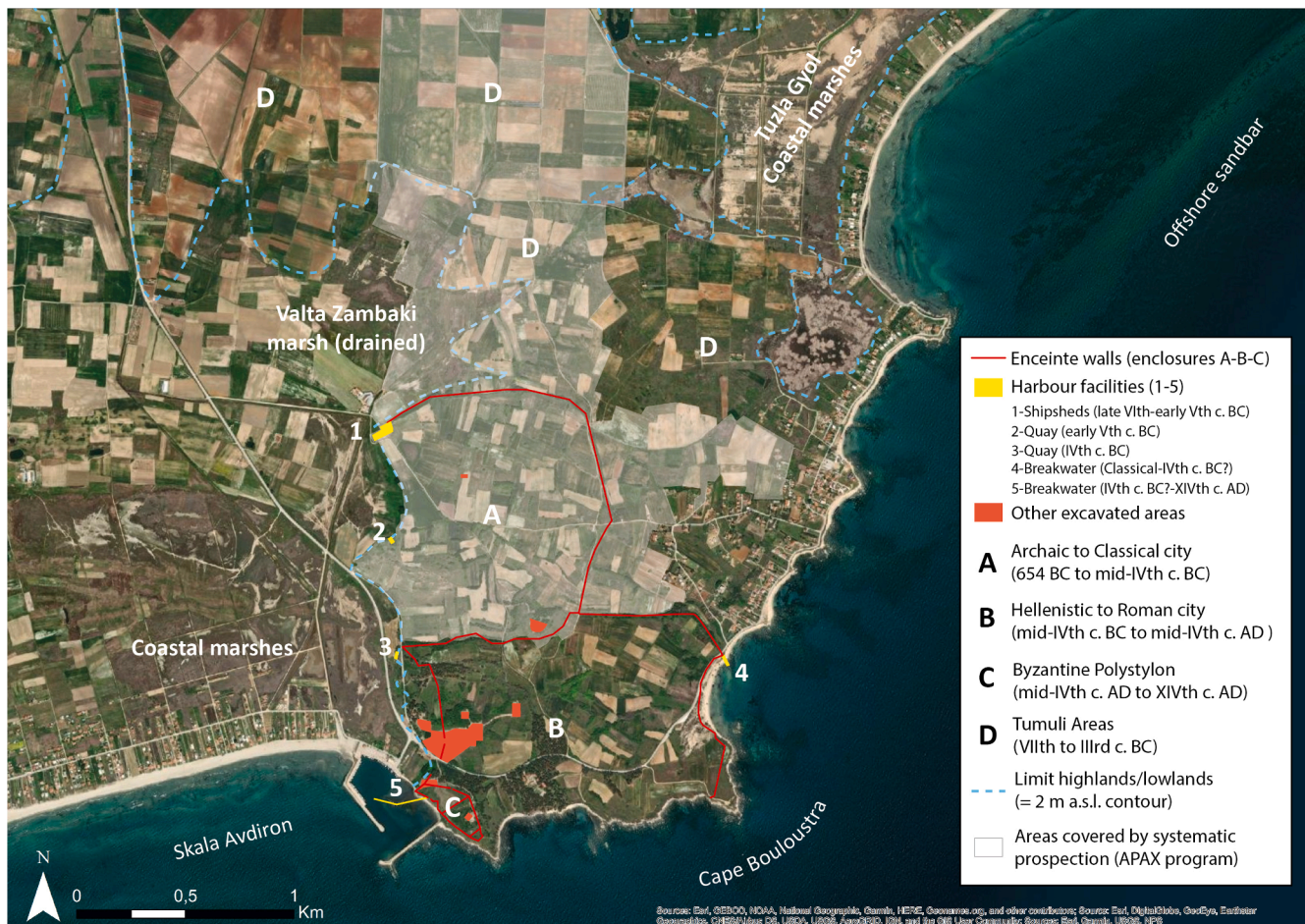
Fig. 3. The main archaeological features of Cape Bouloustra and its surrounding areas. Chronologies from Kallintzi, 2011. Background: Esri World Imagery.

Morhange et al., 2003; Marriner & Morhange, 2007; Vacchi et al., 2016; Koukousioura et al., 2020).

The sedimentary facies and the associated processes and environments were interpreted based on the compiled macroscopic and microscopic evidence, on general geomorphological criteria, coastal geomorphology principles, and on selected references (e.g., Davis et al., 2003; Arche, 2010; Davidson-Arnott, 2010; Fruergaard et al., 2015; González-Villanueva et al., 2015; Devillers et al., 2019; Ruiz-Pérez & Carmona, 2019; Xu et al., 2020). Fig. 4 shows selected examples, and Table 2 provides full descriptions and interpretations. Representative modern analogues were also employed, which were observed in natural profiles, outcrops, and exposures across the study area. Stratigraphic cross-sections and palaeogeographic reconstructions are based on interpretations of these facies over transects of litho-stratigraphic logs, combined with remote sensing, geomorphological mapping, archaeological, and radiocarbon data.

Several cross sections showed layers of washover deposits due to overtopping or breaching of beach-barrier systems by the sea (Goslin & Clemmensen, 2017; Pouzet & Maanan, 2020). They can be attributed to High-Energy Events (HEE) such as intense storms or, less commonly, tsunamis. We used the following criteria to distinguish potential tsunamigenic layers among the rest of the HEE deposits: 1) Lateral and inland extension of hundreds or thousands of meters; 2) deposits homogeneously draping large surfaces instead of infilling existing depressions; 3) features indicative of backflow from the mainland such as floating woody debris and other reworked materials; 4) features indicating very high energy, such as those with a very coarse grain-size and very poor sorting; and 5) specific features such as ripped beach rock fragments and rip-up clasts (Peters & Jaffe, 2010; Engel & Brückner,

2011; Shanmugam, 2012; Engel et al., 2020; Bellanova et al., 2021; De Martini et al., 2021).

3.3. Radiocarbon dating and RSL modelling

A total of 34 samples were sent to various laboratories for AMS radiocarbon dating (Beta Analytics, DirectAMS, Paris-Saclay, and the Arizona Climate & Ecosystems Isotope Lab, see Table 3). Dated materials include marine shells in anatomical connection and living at (or very close to) the water–sediment interface, remains of *Posidonia oceanica* sheaths, terrestrial plant and wood fragments or smaller debris, and charcoal.

Raw dates were calibrated with the Calib v.810 software using the INTCAL20 calibration curve for terrestrial samples and the MARINE20 curve for marine samples (Stuiver & Reimer, 1993; Heaton et al., 2020; Reimer et al., 2020). For the latter we used a DeltaR of -8 ± 40 yr. (Siani et al., 2000). The depths of the samples in Table 3 are raw depths measured directly in the cores, although they were later corrected for decompaction and construction of the composite cores when necessary.

The radiocarbon dataset was also used to reconstruct changes in Relative Sea Level (RSL) in the area, adapting the methodology proposed by Vacchi (Vacchi et al., 2016). However, a more conservative approach was adopted here through the knowledge that all the radiocarbon dates in our sample can only be interpreted as marine lower limiting points, and not directly indicative of RSL.

The corrected depths of 25 selected dates (the 9 aged dates -see Table 3- were not used for RSL reconstruction) were converted into altitude below (current) mean sea level and plotted together on a graph with error bars (age and depth). A sub dataset of 14 samples (10 shells, 4
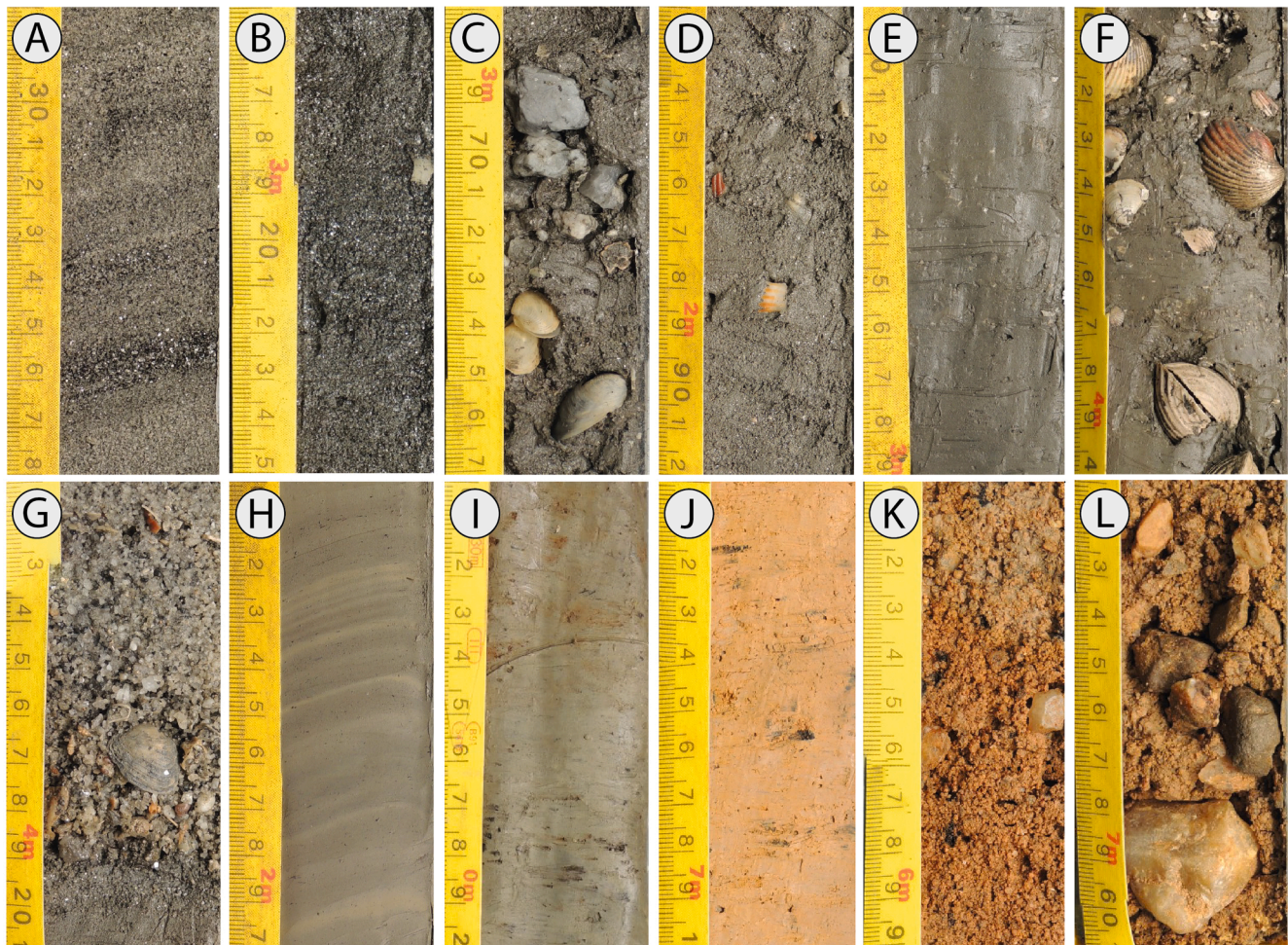
Fig. 4. Selected examples of the main sedimentary facies found in the cores of this study. For details, see the full descriptions in Table 2. A) Beach-Barrier complex: dark grey roughly bedded sands; B) Ancient harbour facies: black silts rich in mica and organic micro-debris; C) Ancient harbour facies: dark grey silty clays with marine shells and marble fragments; D) Open lagoonal: grey sandy clays with shell debris; E) Closed lagoonal: grey massive clays, few shell debris; F) Closed lagoonal: grey clays with marine shells (mainly *Cerastoderma* sp. and *Loripes* sp.); G) Marine High Energy Event: normal-graded coarse grey sands with marine shells and sharp basal contact; H) Coastal pond: massive grey clays with fine laminations and organic micro-debris; I) Marshy: grey clays with organic and oxidation mottles and sparse sand grains; J) Fine alluvial: reddish brown slightly sandy clays with Mn nodules; K) Coarse alluvial: reddish brown medium and coarse sands with few granules and gravels, well-sorted, Mn nodules; L) Coarse colluvial: reddish brown coarse and very coarse sands, poorly sorted, with granules and gravels.

plant samples, see Table 4) was selected to build a curve of estimated Minimal Relative Mean Sea Level (MRMSL). The criteria for selection were the types of sedimentary facies the samples were recovered from, the nature of the samples, ecology of the shells -intertidal to shallow subtidal- (Vacchi et al., 2016), and their consistency with the other limiting points. The rest of the dates (11) were considered subtidal in a broad sense. We added 30 cm to the altitudes of the samples, considering that all were found in aquatic/marine facies -i.e., below some centimetres of water even during low tides- and that the mean tide amplitude in the area is 26 cm (Pavlopoulos et al., 2012). The vertical uncertainty is a sum of the Z precision of the DGPS measurements, the estimated error in depth measurements when coring and posterior corrections for compaction, and the maximum burrowing depth of *Cerastoderma* sp. and *Loripes* sp. shells, that is ~ 5–10 cm (see van der Geest et al., 2011; Anacleto et al., 2016). Two dates from a previous sea-level study in the area (Pavlopoulos et al., 2012) were also recalibrated using the modern standards of this study and incorporated into the final dataset for MRMSL estimation. These dates, a charcoal obtained from a Neolithic shell mound layer and a piece of driftwood associated with marine transgression, were considered to be slightly supratidal and intertidal limiting points respectively (see Ammerman et al., 2008 for details). A polynomic curve was fitted as close as possible to the whole dataset, and

the Mediterranean Sea level of 1950 was also used as an intersection point at 0 cal. BP (Calafat & Gomis, 2009).

4. Results and interpretation

4.1. Geomorphological settings around Abdera

The SMTVI based on Sentinel-2 imagery allows four main types of terrain in the area to be distinguished at a regional scale (Fig. 5 A & B): hilly uplands with dry farming in NE areas representing the horst of Abdera (brownish in A, reddish in B), irrigated coastal lowlands of the Nestos delta in the central and western areas (greenish), the "fresh" alluvium of the Nestos in its active channel (whitish) and a band of coastal deposits with variable width (greyish in A, bluish in B). Many Nestos palaeochannels in the delta and the coastal sand ridge patterns are also clearly visible in both band combinations.

A closer look at the areas to the NE of cape Bouloustra (Fig. 5C & D) shows a clear transition between uplands (brownish in C, reddish in D) and coastal lowlands (greyish/bluish), in large part flooded (black). These wetlands that stretch eastwards from the colony are separated from the open sea by a large beach-barrier extending out in a SW/NE direction. By contrast, moving westwards from the colony the transition
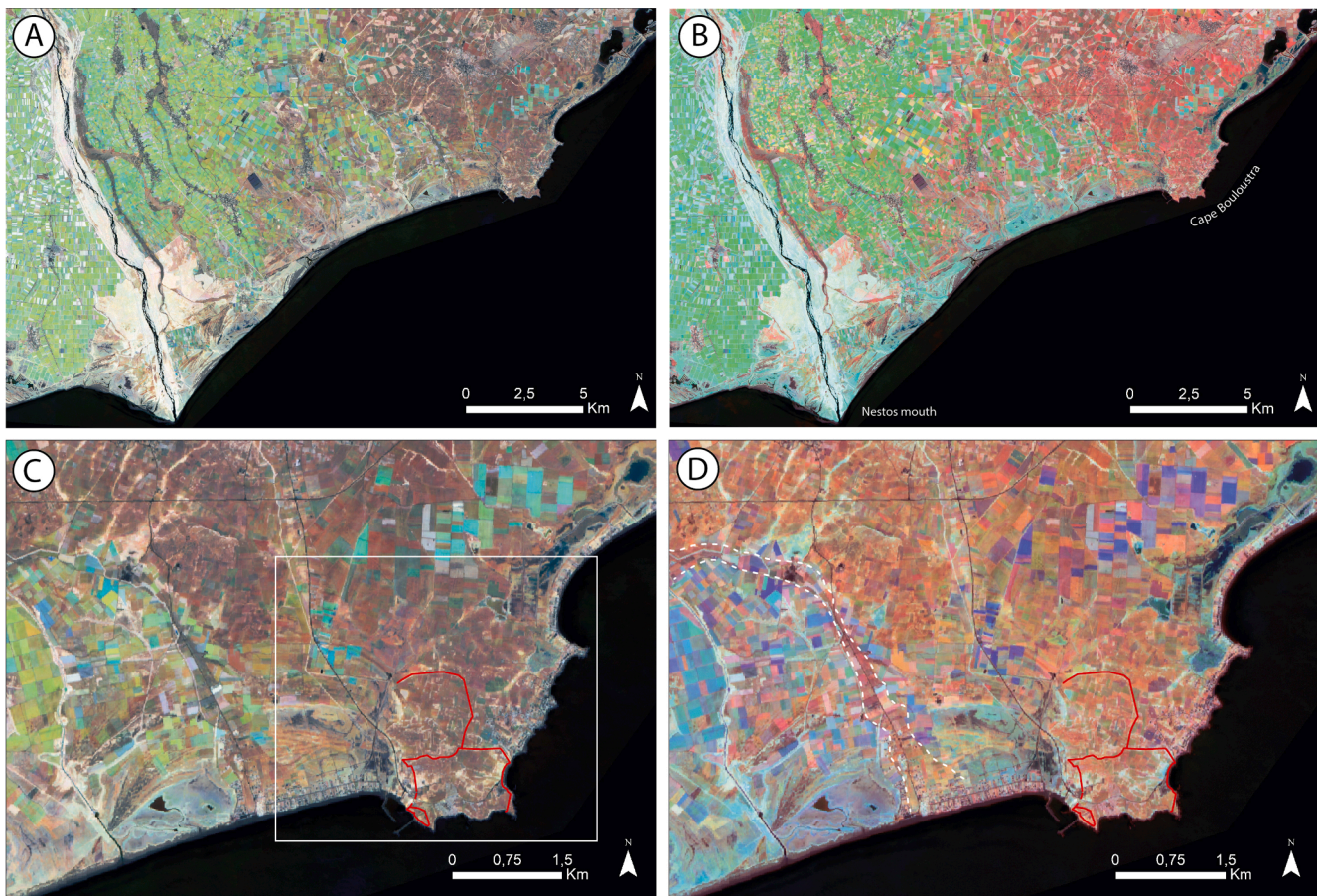
Fig. 5. The different Sentinel-2 SMTVI band combinations (see Orengo & Petrie, 2017 for details) of the region between the Nestos River and cape Bouloustra (A, bands 345, and B, bands 245), and the area around the cape itself and the Greek colony (C, bands 345, and D, bands 234). The white frame in C represents the coverage of the geomorphological mapping (Fig. 6). White dashed lines in D mark a recent palaeochannel of the Nestos cross-cutting all the previous landforms in the lowlands west of the cape. The enceinte walls of both the Greek cities and the Polystylon are marked in red (See Fig. 3 for details). (For interpretation of the references to colour in this figure legend, the reader is referred to the web version of this article.)

between dry highlands and extensive wet lowlands is gradual and diffused, suggesting that their inner parts may be higher and drier. Several generations of sandbars formed by thick accumulations of numerous sand ridges can be distinguished, which are separated by lower and wetter areas (or partly flooded in some sectors). Finally, a large palaeochannel of the Nestos seems to have cross-cut all these landforms in relatively recent times (Fig. 5D).The geomorphological map shows the landforms and superficial deposits around the colony as they were before the land reclamation projects of the mid-20th c. (Fig. 6). The coast of the promontory itself is rocky overall, with small cliffs, abundant reefs, and narrow, discontinuous sandy beaches. The rest of the areas of the littoral are sandy, with abundant offshore sandbar ridges visible in aerial imagery. Coastal lowlands to the NE of the promontory of Abdera are dominated by seasonally wet salt marshes, sand flats, and mudflats, i.e., the "Tuzla Gyol marsh" (Fig. 6). Two sectors can be distinguished: a small wetland area almost completely surrounded by higher terrain in the southern extreme of the marsh, and a larger body of wetlands which continues northwards outside the extent of the study area. Both are connected by a narrow "neck" and are separated from the open sea by a thick beach-barrier (n°1-7, Fig. 6). A narrow fossil sandbar (n°0, Fig. 6) separates the Tuzla Gyol wetlands from the inner areas of the coastal lowlands, which are slightly higher and much smaller.

In the vast lowlands to the W and NW of the colony, the situation is clearly different. The inner and higher parts of the coastal plain are occupied by dry and bushy salt marshes, sand flats, and mud flats located in large headwater areas that are in contact with the highlands

(e.g., the Valta Zambaki area, Fig. 3). They are separated of the lower, more external areas of the coastal plain by a very thick complex of several fossil sandbars and beach-barriers, which can be assimilated to a small strandplain (n° 1–3 in Fig. 6). A depression with seasonally wet salt marshes, sandflats, and mudflats separates this ensemble from a second and more complex one (n° 4a-c, 5 and 6 in Fig. 6). The latter is composed of fragments of sandbars and beach-barriers which take different directions and form different patterns suggesting changes in the configuration of the coastline. In the same area, a small and mound-shaped gneiss outcrop (marked in red silhouette in Fig. 6) represents an ancient landlocked islet which was certainly surrounded by reefs. A second and large depression occupied by seasonally wet salt marshes, mud flats, and sand flats lies between sandbar n° 6 and the current beach barrier system (n°7, see Fig. 6). The whole area is cross-cut by a recent palaeochannel of the Nestos river (see also Fig. 5).

4.2. Stratigraphic cross-sections in the western lowlands, the Valta Zambaki marsh and the Archaic harbour area

The stratigraphic cross-section of Transect 1 (T1) cuts across all the main accumulative landforms of the western side of the colony (Fig. 6). The base sections of cores AVZ1 and AVZ3 show clayey, low-energy alluvial facies that clearly correspond to floodplain deposits derived from reddish soils of the surrounding gneissic hills. They are followed in AVZ1 by higher energy sandy facies, representing instead channel deposits of a low-order stream. Superimposed pedogenic features point to phases of morphogenic stability with alternating wetter and drier
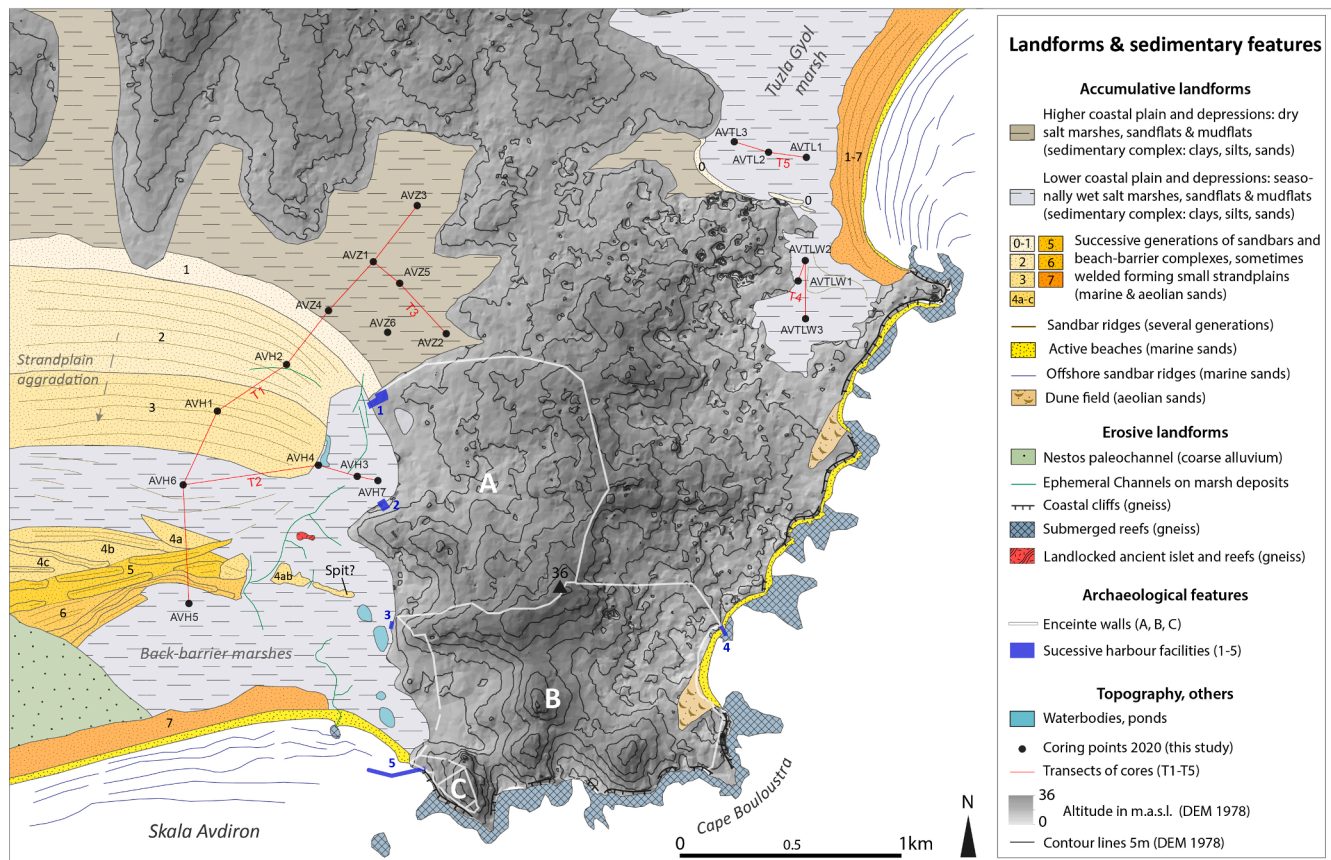
Fig. 6. Geomorphological map of the coastal lowlands in the study area before the 1950′s, including the main archaeological features and the position of the stratigraphic cross-sections along transects T1-5.

conditions (Mn nodules vs. leaching and illuviation/precipitation features). These facies are covered by an incipient brownish soil that dates to before c. 4847 cal. BC (Fig. 7). Its upper part is reduced and overlaid by much finer greyish anoxic sediments including a fragment of man-made Late Neolithic fired clay. This facies certainly represents a short-lived transition phase, with a rise of the water table before the maximal extension of the Holocene marine transgression around c. 5000 cal. BC, as shown by the overlying lagoonal facies. From this date onwards, a shallow lagoon with very quiet waters (heavy clays; several low-stands and an emersion phase) developed in the Valta Zambaki area, which was only disturbed by a marine HEE just before c. 2000 cal. BC (AVZ4). This suggests that the lagoon was isolated from the open sea by a well-developed beach-barrier (n°1, Figs. 6 and 7), that definitely still represented the active coastline by c. 650 cal. BC as based on the archaeological data (Klazomenian ship sheds, Fig. 3). By then, the Valta Zambaki lagoon had silted up and was a marsh with dry margins (Fig. 7). A second washover deposit (AVZ4) suggests that in the centuries that followed intense storm activity may have temporarily increased the connection the marsh had with the sea and its water depth.

Radiocarbon dates in the seabed facies at the base of AVH1 and AVH2 suggest that by the 4th c. BC the water depth was relatively shallow in front of beach-barrier 1 (≥1.75 m, considering an RSL of −60 cm for this period - Pavlopoulos et al., 2012). Coastal progradation was certainly only incipient, if at all existent, at this time, and the massive beach-barriers 2 & 3 grew later in Hellenistic and Roman times (3rd c. BC to mid-2nd c. AD), through the thickening and accretion of beach-barrier 1. Dates taken from AVH6 and AVH4 indicate that by 150 cal. AD the coast had advanced even more and beach-barrier 4 was already closed (see Figs. 6, 7 and 8). Beach-barriers 5–6 did not prograde significantly after this date but maintained a small back-barrier pond (AVH4 and 6, Figs. 7 & 8) that was affected by massive sandy washovers

and ultimately became a seasonal marsh. By this period, Valta Zambaki was a salt marsh that was almost completely silted up and disconnected from the sea (c. 310 cal. AD in AVZ1), with marked emersion episodes and even fine colluvial deposits in later phases. These were covered by sandy layers of a HEE (Fig. 7, AVZ1 & AVZ3), after which the area evolved into a dry coastal plain with ephemeral pools.

The last beach-barrier system (n°7, see Figs. 6 and 7) seems to have developed from Late Antiquity onwards, considering the position of the harbour of the Byzantine Polystylon (Figs. 3 and 6), and remained without major changes until the present-day. Marshy areas, mudflats, and sandflats developed in the back-barrier space, and were affected by 3–4 HEEs from the Byzantine to modern period reflecting washover episodes and flooding that were most likely caused by intense storms (AVH5 in Fig. 7).

Transect 3 confirms and complements the interpretations of the data from T1 in the Valta Zambaki marsh (Fig. 8B). The bases of cores AVZ2 and AVZ5 support the existence of an ancient thalweg before ∼ 4850 cal. BC centred in core AVZ1 and filled with alluvial sediments. After the marine transgression, the lagoonal low-stands or short emersions were more frequent and marked in AVZ5 than in AVZ1 (the depocenter of the lagoon), whereas marshy conditions always prevailed in AVZ2. Later marshy and dry phases detected in AVZ1 also extended to AVZ2 and AVZ5, showing that the trend towards emersion was persistent in Antiquity and that marshes were widespread throughout the Valta Zambaki area. Remarkably, the sandy layers covering these facies are also very widely extended, reinforcing the idea of an extensive HEE that occurred after c. 310 cal. AD.

The stratigraphic cross-section of Transect 2 (Fig. 8A) depicts a more complex situation in the areas close to the ship sheds of the Archaic colony (cores AVH3 & AVH7). The oldest sedimentary facies are reddish colluvial and alluvial deposits at the base of AVH7, which clearly

Table 2

Detailed lithological and pedo-sedimentary description of the sedimentary facies found in the cores of this study, with an interpretation of the associated depositional environments and processes.

Sedimentary facies	Main lithological and pedo-sedimentary features	Associated depositional environments and processes
Marine - High Energy Event	Grey, dark grey or brownish grey medium to coarse sands in layers of variable thickness, with sparse granules and gravels. Occasionally fine sands or very coarse sands to granules and gravels (subangular and angular). Finer layers are well sorted and sometimes roughly bedded. Coarser layers are poorly or very poorly sorted, show often normal grading (fining-up), and rarely reverse grading. In some cases, there are sharp basal erosive contacts. Inclusions of ripped beachrock fragments are found along with very rounded pottery sherds and rip-up clasts. Marine shells are sometimes absent (clean sand), but in some cases are abundant including *Cerastoderma* sp., *Cerithium* sp. and juvenile *Bitthium sp.* among others, and much shell debris, some of which is very rounded. Locally, very abundant driftwood and organic remains.	Marine High-Energy Events, either storm surges or tsunami, resulting in overtopping/breaching of beach-barriers: proximal and distal washover fans, high energy wave deposits, backflow deposits.
Beach-Barrier complex	Dark grey (waterlogged) and beige or brown (dry) fine to medium sands, sometimes coarse sands, and more rarely very fine silty or even clayey sands. Extremely well sorted and homogeneous, most often massive although sometimes roughly bedded. Occasional organic remains (e.g., wood, vegetal fibres, micro-debris), and rare marine shells (*Loripes* sp.*, Donax* sp.). Locally remains of *Posidonia oceanica* sheaths. Oxidation mottles at the intersection with the water table.	Marine littoral and coastal sands, including shallow seabed, sandbars, beach sands, sandflats, dunes and windblown sand sheets
Open lagoonal	Bluish grey to grey/dark grey silty and sandy clays, often with coarser sands, and granules, less commonly small gravels, and much small shell debris. Many marine shells including *Cerastoderma* sp., *Loripes* sp.*, Cerithium sp.*, *Bittium sp.*, *Abra sp.*, *Tritia sp.* and *Trochidae*, among other secondary taxa such as *Donax sp.* and *Natica sp*. Very locally, remains of *Posidonica oceanica* sheaths.	Open lagoons and very sheltered bays or inlets, with marked sedimentary influx from the open sea and beach-barriers.
Closed lagoonal	Bluish grey to grey/dark grey, or brown or greyish brown (if subject to post-depositional oxidation) massive clays, sometimes slightly silty or sandy. Variable amounts of marine shells and shell debris, from few to extremely abundant, dominated by *Cerastoderma* sp., secondarily by *Cerithium sp.* and *Loripes* sp., and other ancillary taxa such as *Bittium* sp.*, Tritia* sp. or *Trochidae*. Few organic remains, rarely rootlets. Occasionally several to abundant oxidation mottles.	Very low-energy, closed lagoons, with very little sedimentary influx from the open sea and beach-barriers. Sometimes evolving to very shallow or almost marshy conditions during low-stand phases, or even short emersions.
Coastal pond	Grey clays, sometimes slightly silty or very fine sandy. Abundant fine laminations, alternating darker, slightly coarser and more organic laminae with lighter, finer pure clay laminae. Abundant organic micro-and macro debris (terrestrial vegetal remains), total absence of marine shells.	Low-energy coastal ponds fed by runoff. Alternating slight detrital influx with local clay decantation.
Marshy	Black, dark grey, grey, brown or light brown clays and silty clays, sometimes slightly sandy, with very sparse coarser particles. Occasionally silty or fine sandy beds. Frequent vegetal micro-debris, amorphous organic dots, and rootlet traces. Frequent to locally abundant oxidation mottles, few Mn nodules. Few to very few marine shells, mainly debris of *Cerastoderma* sp.	Permanent or seasonal back-barrier (salt) marshes, marshy borders of lagoons and mudflats. Commonly pedogenized. Sandbar or alluvial sedimentary influx.
Coarse alluvial	Reddish brown and brown medium sands to gravels, sometimes slightly clay enriched. Moderately to well-sorted, occasional fining-up layers. Frequent oxidation mottles, Mn nodules, beige precipitates and root traces.	High-energy channel or bar deposits of small streams. Incipient pedogenesis.
Fine alluvial	Reddish brown clays, sometimes slightly silty or sandy, more rarely with sparse granules and gravels. Occasionally Mn nodules, beige precipitates and root traces.	Low-energy distal floodplain deposits, incipient pedogenesis.
Fine colluvial	Grey, beige or brown silty clays to silty very fine sands, arranged in beds up to 20 cm thick. Occasionally fine to medium sands, with normal grading. Moderately to well sorted, rare sparse granules and gravels. Few to several rootlets and organic remains. Occasionally Mn nodules and oxidation mottles close to the water table.	Dry sandflats and mudflats reworked by rainwash and diffuse runoff, with local muddy puddles, and often pedogenized
Coarse colluvial	Reddish brown to brown coarse and very coarse sands, very abundant granules and gravels up to 4 cm. Very heterometric and poorly sorted. The coarsest particles have a varied lithology and are mainly subangular to subrounded.	Gravitational deposits, reworking older alluvial, slope deposits or palaeosoils. Some pedogenized.
Weathering profile	Reddish brown to brown granules and gravels, with sandy mica-rich matrix, and little silts and clays, very heterometric. The coarsest particles are gneissic, subangular to angular, and show clear oxidation, weathering, and disaggregation. Grain-size increases, weathering, and matrix decrease downwards. Few Mn nodules.	Weathering profile, developed in subaerial conditions (base of palaeosoils) on gneiss bedrock.
Ancient harbour parasequence (Marriner & Morhange, 2006)	Very dark grey to black silty clays to silty very fine sands, rich in mica. Well-sorted, with very rare granules and gravels. Abundant organic remains and micro-debris, and several human artefacts such as carved wood or marble. Reverse grading (coarsening-up) at the scale of the sequence, with development of faint laminae. Several marine shells downwards (*Loripes* sp.*, Mytilus galloprovincialis*, among others), but rare or absent upwards.	Sequence representing an ancient harbour basin foundational surface, its functioning, and posterior silting in low-energy conditions.
Anthropogenic	Brown and reddish brown clays to coarse sands, with mottled, mixed, and reworked aspect. Very heterogeneous texture with many inclusions of granule to- gravel-sized particles and marine shell fragments (reworked).	Modern artificial backfill for land reclamation in low-topography marshy areas.

Table 3

Radiocarbon dating results. *Italic: aged (not used for chrono-stratigraphic interpretation and for RSL reconstruction)*; *: rejected.
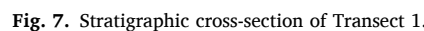
N°	Lab code	Core	Raw depth (cm)	Composite depth (cm)	Material	δ13C	14C yr. BP	Cal yr. BC/AD (INTCAL20 or MARINE20 with ΔR −8 ± 40 yr.)	Cal yr. BC/AD (INTCAL20 or MARINE20 with ΔR −8 ± 40 yr.; Median)
1	Beta − 566000	AVZ-1b	524.5	527	Shell-Cerastoderma sp.	−1.2o/oo	6510 ± 30	5037–4658 cal. BC	4847 ± 189 cal. BC
2	Beta − 566001	AVZ-1b	237.5	239	Shell-Cerastoderma sp.	−1.5o/oo	3010 ± 30	839–470 cal. BC	654 ± 184 cal. BC
3	Beta − 566002	AVTL-1b	333.5	334	Shell-Cerastoderma sp.	+1.6o/oo	6510 ± 30	5037–4658 cal. BC	4847 ± 189 cal. BC
4	Beta − 566003	AVTL-1b	530	554	Shell-Cerithium sp.	+1.9o/oo	6790 ± 30	5332–4974 cal. BC	5153 ± 179 cal. BC
5	Beta − 566004	AVTLW-2b	257.5	257.5	Shell-Cerithium sp.	+2.4o/oo	6140 ± 30	4609–4259 cal. BC	4434 ± 175 cal. BC
6	Beta − 566005	AVTL-1b	174.5	187	Shell-Cerastoderma sp.	−0.2o/oo	5040 ± 30	3441–3015 cal. BC	3228 ± 213 cal. BC
7	D-AMS 040365	AVZ-1c1	159	153.5	Wood/plant	N/A	1752 ± 23	241–376 cal. AD	308 ± 67 cal. AD
8	*D-AMS 040366*	*AVH4*	*141*	*141*	*Wood*	*N/A*	*2238 ± 24*	*386–204 cal. BC*	*295 ± 91 cal. BC*
9	D-AMS 040367	AVH4	293	293	Plant debris	N/A	1854 ± 21	128–235 cal. AD	181 ± 53 cal. AD
10	D-AMS 040368	AVH6	229	229	Wood/plant	N/A	1921 ± 22	29–206 cal. AD	117 ± 88 cal. AD
11	*D-AMS 040369*	*AVH7*	*156.5*	*154.5*	*Wood*	*−26.31o/oo*	*2363 ± 26*	*536–389 cal. BC*	*462 ± 73 cal. BC*
12	*D-AMS 040370*	*AVH7*	*245*	*243*	*Charcoal*	*−25.26o/oo*	*2413 ± 24*	*731–403 cal. BC*	*567 ± 164 cal. BC*
13	D-AMS 040371	AVH7	245	243	Posidonia sheaths	−10.94o/oo	2456 ± 23	167 cal. BC-197 cal. AD	15 ± 182 cal. AD
14	D-AMS 040372	AVH7	349.5	348.5	Wood	N/A	2404 ± 23	718–401 cal. BC	559 ± 158 cal. BC
15	D-AMS 040373	AVH7	418	418	Posidonia sheaths	−11.89o/oo	2952 ± 22	774–423 cal. BC	598 ± 175 cal. BC
16	D-AMS 040374	AVTL-1c1	79	60	Charcoal	−25.34o/oo	1650 ± 22	265–534 cal. AD	399 ± 134 cal. AD
17	D-AMS 040375	AVH7	156.5	154.5	Shell-Loripes sp.	+0.43o/oo	2372 ± 25	61 cal. BC-300 cal. AD	120 ± 180 cal. AD
18	D-AMS 040376	AVTLW-3b1	73	73	Shell-Cerastoderma sp.	−0.42o/oo	2642 ± 21	383–45 cal. BC	214 ± 169 cal. BC
19	D-AMS 040377	AVTLW-3b1	185.5	185.5	Shell-Cerastoderma sp.	+2.29o/oo	4399 ± 25	2612–2212 cal. BC	2412 ± 200 cal. BC
20	D-AMS 040378	AVTLW-3b1	379.5	379.5	Shell-Cerastoderma sp.	1.46o/oo	6593 ± 27	5143–4744 cal. BC	4943 ± 199 cal. BC
21	*Beta − 582846*	*AVZ-1b*	*180*	*182*	*Residual OM*	*−26.0o/oo*	*4910 ± 40*	*3775–3637 cal. BC*	*3706 ± 69 cal. BC*
22	NAU2403	AVZ-4	312	312	Wood	N/A	3630 ± 20	2122–1927 cal. BC	2024 ± 97 cal. BC
23	NAU2405	AVH3	429	429	Wood/plant/leaf	N/A	1880 ± 15	122–215 cal. AD	168 ± 46 cal. AD
24	NAU2406	AVH2	355	355	Wood	N/A	2275 ± 15	394–232 cal. BC	313 ± 81 cal. BC
25	NAU2407	AVH1	419	419	Wood	N/A	2320 ± 15	403–384 cal. BC	393 ± 9 cal. BC
26	Beta-620752	AVH4	152	152	Plant debris	−28.3o/oo	1760 ± 30	234–381 cal. AD	307 ± 74 cal. AD
27	Beta-620753	AVH4	240	240	Plant debris	−29.1o/oo	1720 ± 30	250–412 cal. AD	331 ± 81 cal. AD
28	*Beta-620755*	*AVZ-1c2*	*253.5*	*252*	*Shell-Cerastoderma sp.*	*−4.3o/oo*	*2980 ± 30*	*802–442 cal. BC*	*622 ± 180 cal. BC*
29	*Beta-620756*	*AVH7*	*270.5*	*269.5*	*Woody material*	*−26.1o/oo*	*N/A*	*1892–1957 cal. AD*	*1924 ± 32 cal. AD*
30	Beta-620757	AVH7	295	295	Shell-Loripes sp.	+1.8o/oo	2520 ± 30	281 cal. BC-128 cal. AD	76 ± 204 cal. BC
31	Beta-623455	AVZ-1c2	253.5	252	Plant debris	−24.3o/oo	3180 ± 30	1505–1408 cal. BC	1456 ± 48 cal. BC
32	*SacA-66052*	*AVH3*	*144*	*144*	*Wood*	*N/A*	*1955 ± 30*	*39 cal. BC–200 cal. AD*	*80 ± 120 cal. AD*
33	*SacA-66053*	*AVH3*	*180*	*180*	*Wood*	*N/A*	*1915 ± 30*	*27–212 cal. AD*	*120 ± 92 cal. AD*
34	*SacA-66054*	*AVH3*	*232.5*	*232.5*	*Driftwood (rounded)*	*N/A*	*2205 ± 30*	*371–175 cal. BC*	*273 ± 98 cal. BC*

developed before the 5th millennium cal. BC (as shown by stratigraphic correlation with AVZ1, Figs. 7 and 8B). Remarkably, the short transition facies just before the transgression also includes a piece of Late Neolithic fired clay just as it did in AVZ1. The marine invasion is more sharply marked here by the sudden deposition of medium to coarse sands with marine malacofauna. This relatively high-energy environment seems to have prevented any significant seabed accretion in the following millennia (Fig. 8A).

The overlying layer developed from c. 600 cal. BC: its significantly finer facies with sandy silts and many remains of *Posidonia oceanica* suggests an environment akin to a very sheltered bay (Votruba, Artzy, & Erkanal, 2016; Abadie et al., 2018). A little later in the 6th c. cal. BC, a more abrupt facies change is evident in AVH7: sandy silts give way to silty clays with abundant organic matter and anthropogenic artifacts such as marble or carved wood. This indicates a very low-energy sedimentary environment isolated from the open sea and under the direct

Table 4

Radiocarbon dataset used for MRMSL reconstruction in the area of Abdera and Cape Bouloustra. Samples 70A and 70B from Ammerman et al., 2008 and Pavlopoulos et al., 2012, recalibrated. See the main text for details.

N°	Sample code (core / Site)	Depth (cm)	Corrected alt. below current sea-level (cm)	Dated material	Sedimentary facies	Age yr. cal. BP (2σ)	Indicative value
1	AVZ-1b 524–525	527	−400 ± 10	*Cerastoderma*	Transition alluvial- open lagoonal (marine transgression)	6797 ± 189	Intertidal or slightly subtidal
2	AVZ-1b 237–238	239	−112 ± 10	*Cerastoderma*	Shallow closed lagoonal to marshy	2604 ± 184	Intertidal to subtidal
3	AVTL-1b 333–334	334	−299 ± 10	*Cerastoderma*	Open lagoonal	6797 ± 189	Intertidal to subtidal
4	AVTL-1b 530	554	−519 ± 7.5	*Cerithium*	Closed lagoonal	7103 ± 179	Subtidal
5	AVTLW-2b 257–258	257,5	−196 ± 7.5	*Cerithium*	Closed lagoonal	6384 ± 175	Subtidal
6	AVTL-1b 174–175	187	−152.5 ± 10	*Cerastoderma*	Closed lagoonal	5178 ± 213	Intertidal to subtidal
7	AVZ1C1 158–160	153.5	−26.5 ± 7.5	Wood/plant	Shallow closed lagoonal to marshy	1642 ± 67	Likely intertidal
16	AVTL1C1 52–54	60	−25 ± 7.5	Charcoal	Shallow closed lagoonal	1551 ± 134	Likely intertidal
17	AVH7 156–157B	154.5	−46 ± 12.5	*Loripes*	Ancient harbour facies to marshy	1830 ± 180	Subtidal
18	AVTLW3B1 73	73	−32 ± 10	*Cerastoderma*	Closed lagoon to marshy	2164 ± 169	Intertidal to subtidal
19	AVTLW3B1 185–186	185.5	−145 ± 10	*Cerastoderma*	Closed lagoon	4362 ± 200	Intertidal to subtidal
20	AVTLW3B1 379–380	379.5	−339 ± 10	*Cerastoderma*	Closed lagoon	6893 ± 199	Intertidal to subtidal
26	AVH4 152	152	−46 ± 7.5	Plant debris	Coastal pond	1643 ± 74	Intertidal to subtidal
31	AVZ-1C2 253–254 A	252	−125 ± 7.5	Plant debris	Shallow closed lagoonal to marshy	3406 ± 48	Likely intertidal
70A	LAFROUDA A	–	−250 ± 30	Charcoal	Archaeological layer	6976 ± 180	Supratidal
70B	LAFROUDA B	–	−60 ± 30	Driftwood	Marine transgression	2864 ± 82	Intertidal

Fig. 7. Stratigraphic cross-section of Transect 1.

influence of the Archaic colony. Posterior accumulation of roughly laminated, organic and mica-rich sediment, which becomes gradually coarser moving upwards, occurs surprisingly fast from the 1st c. cal. BC. Simultaneously, marine malacofauna becomes rare and macroscopic markers of anthropic activity disappear. Radiocarbon dates here yield different chronologies for paired dates (see Fig. 8A and Table 3): shells and *Posidonia* sheaths provide younger dates, whereas wood and charcoal show aged dates most likely related to inputs from the Archaic city soils. After 120 cal. AD, a couple of brownified layers show that the area was emerging. All these features of AVH7 are compatible with the so-called "ancient harbour facies" (Marriner & Morhange, 2006), which is also consistent with the location of the core sample taken from what was certainly the harbour area of the Archaic-Classical city (Figs. 3 & 6).

Meanwhile, the area immediately westwards from AVH7 (cores AVH3, 4 and 6) had been open sea since the mid-Holocene transgression. The extremely abrupt lateral facies change between AVH7 and AVH3-4–6 at a distance of only 95 m, and the lack of older sediments in these cores, suggest that a sharp morpho-sedimentary barrier, either natural or anthropogenic, existed between AVH7 and AVH3. From the 1st c. AD until 150 cal. AD, the beach-barrier complex 3 (see Figs. 6 and 8) had prograded significantly shallowing this area of the embayment, whereas open lagoonal conditions had developed in AVH3. Circa 170–180 cal. AD a new sand body, probably a part of beach-barrier 5, had isolated AVH6 and AVH4 from AVH3. Laminated clay deposition occurs in the first two cores from the end of the 2nd to the 4th c. AD, confirming the presence of a coastal pond as suggested by Transect 1 (Fig. 7). This pond records a couple of HEEs during the 3rd or 4th c. cal. AD (AVH6 and AVH4, Fig. 8A), although their limited extension and intensity suggest they were likely sandy washovers caused by storms. Simultaneously, the

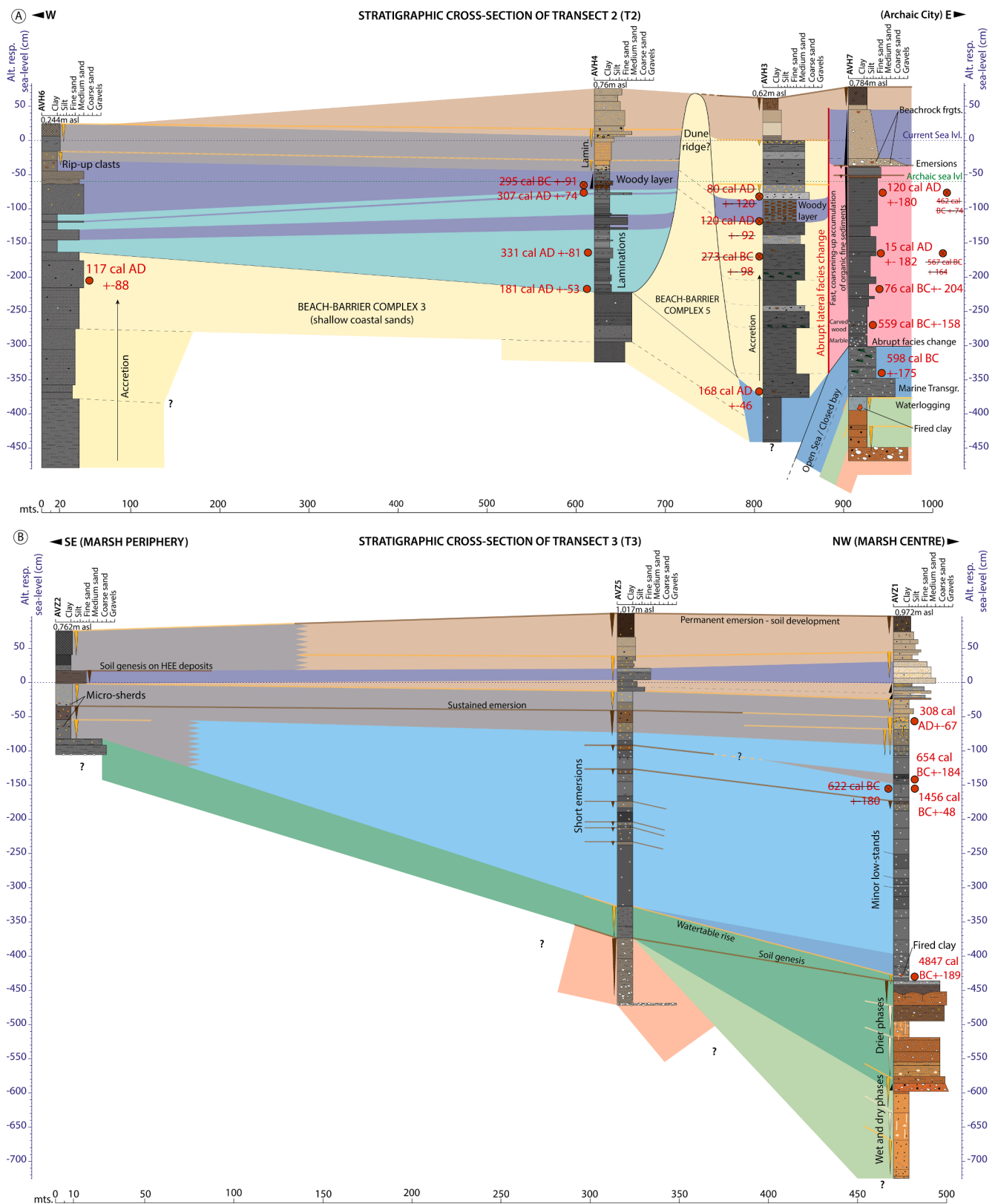presence of sands with *Posidonia* remains in AVH3 suggests the presence of a narrow, calm, and shallow sea inlet that was gradually infilled by the accumulation of marine sediments. A radiocarbon date of 273 ±98 cal. BC taken from a piece of rounded driftwood is clearly very aged here, as it is in marked inversion with the date at the base of the sequence. All these deposits in AVH6, AVH4 and AVH3, along with those from the top of the laminated facies in AVH7, are covered by a high-energy deposit which clearly corresponds to a single HEE. In AVH4 and AVH3 it appears as a layer that is extremely rich in woody debris (Fig. 8A). Several dates in this "woody layer" yielded different ages between 295 cal. BC and 120 cal. AD, all inverted with other dates in the sequences, suggesting that these wood fragments were certainly reworked by a HEE with backflow processes (Bellanova et al., 2021). In contrast, these HEE deposits appear as thick sandy layers including rip-up clasts in AVH6 and AVH7, and in the latter marine shell debris, rounded sherds, and beach-rock fragments are also found (Fig. 8A). This HEE is clearly the strongest and most significant of all the analysed stratigraphic sequences. Indeed, it appears in the first 1–1.5 m of 9 cores in the west side of the Abdera promontory (AVZ1, 2, 3, 5, 6; AVH3, 4, 6, 7; Figs. 7 and 8). This HEE layer, that largely exceeds the extension and intensity of typical washover deposits in the area, is roughly dated in AVH4 after c. 310 cal. AD. Seasonal marshy conditions develop hereafter as seen in cores AVH6 and AVH4, and the sea inlet in AVH3 is clogged by sandy deposits. The area finally becomes a dry, sandy, coastal plain with occasional floods and ephemeral pools.

Fig. 8. Stratigraphic cross-sections of Transects 2 and 3. The legend is the same than in Fig. 7.

4.3. Stratigraphic cross-sections in North-Eastern wetlands (Tuzla Gyol area)

Stratigraphic cross-sections 4 and 5 cover the Tuzla Gyol marsh (Fig. 9, see also Fig. 6). The bases of the cores in T4 (southern sub-basin),

which are slightly coarser (sandy clays or sands) than the rest of the sequences, are consistent with an open lagoon facies (Fig. 9A). These are overlaid by heavy clays rich in malacofauna, suggesting the onset of a low-energy, closed lagoon environment from c. 4950 cal. BC onwards. These dates are roughly consistent with the marine transgression dated

in core AVZ1 to the beginning of the 5th millennium BC (Figs. 7 and 8). This quiet and very stable closed lagoon is maintained over several millennia, but by 214 cal. BC it has become very shallow and is almost completely silted up. In the centuries that follow, the lagoon is even affected by a period of sustained emersion as shown by a strongly brownified horizon (Fig. 9A). This dryer phase is followed by wetter marshy or very shallow lagoonal conditions, and finally by a very shallow seasonal marsh that has lasted until the present day.

The northern sub-basin, which is much larger than the southern one, is covered by Transect T5 (Fig. 9B, see also Fig. 6) and shows a more complex sedimentary history. The deepest levels in core AVTL1 correspond to alternating coarse alluvial and colluvial deposits, with a phase of stability marked by incipient pedogenesis of the upper colluvial layer. The second alluvial layer is affected by reduction that is certainly due to the contemporaneous rising of the sea-level and the progress of the aforementioned marine transgression. This is confirmed by the sudden deposition of fine, heavy lagoonal clays with marine malacofauna which occurred shortly after and continued from c. 5150 cal. BC onwards (Fig. 9B). During an initial phase a small, closed lagoon with a very low-energy environment coexists with marshy conditions in other inland areas. However, this is quickly followed from the beginning of the 5th millennium BC (c. 4850 cal. BC) by a rather open lagoonal environment, including several, and sometimes thick, sandy layers. Sands are often arranged in fining-upwards sequences, with sharp inferior contacts and coarse to very coarse grain sizes, sometimes even with small gravels. The malacofauna in these layers is also more variegated than in the clayey lagoonal facies, indicating increased connectivity with the sea. All these features are especially marked in the core closest to the sandbar (AVTL1, see Fig. 9B and Fig. 6). They indicate strong -although limited in extent-washover phenomena into the lagoon, which are likely due to a succession of up to 6 HEEs. These episodes most likely represent intense storms that had enough energy to breach or overtop the beach-barrier system occurring some time during the 5th and 4th millennium cal. BC.

Sedimentary conditions change again at c. 3230 cal. BC. From this date onwards, the three cores are dominated by heavy clays characteristic of a low-energy, closed lagoonal environment with abundant malacofauna. By c. 400 cal. AD, the lagoon was certainly very shallow and almost completely silted up. Immediately after this date, a very marked sandy layer appears in core AVTL1, similar to those found in the western areas of the colony, suggesting a washover due to a HEE (Fig. 9B, see also Figs. 7 and 8). Its chronology and stratigraphic position suggest that this HEE is the same as the one recorded in the upper parts of the 9 cores in Valta Zambaki and the Archaic harbour areas (see 4.2). This event could have temporarily enhanced the connection of the area with the sea, as the overlying facies suggests a slight increase of the water depth in the lagoon when compared to the previous centuries (similar to the top of cross-section 4, Fig. 9A). However, the long-term trend towards silting and shallowing quickly resumed: the waterbody seems to finally dry up, and a seasonal marsh remained in core AVTL2 until the land reclamation works of the 1990′s.

5. Discussion

5.1. Middle- to Late Holocene Relative Sea-Level changes in the Cape Bouloustra area

Fig. 10 shows the Minimum Relative Mean Sea Level (MRMSL) curve from 7250 cal. BP reconstructed using a subset of radiocarbon dates obtained in this study as marine limiting points (Table 4). Two recalibrated dates from a Neolithic shell mound located 5 km NE of Abdera close to the Lafrouda lagoon (see Ammerman et al., 2008; Efstratiou, 2016) have also been added. The polynomial MRMSL curve fits the whole dataset well ($R^2 > 0,95$). Considering that our marine limiting points are mostly intertidal to slightly subtidal, we argue that our reconstruction is accurate and that the exact RMSL was very close -likely only a few centimetres- above the MRMSL curve. This is also supported

by the consistency our dataset shows with the two previous dates from the Lafrouda Neolithic shell mound (Ammerman et al., 2008). Even though the group of dates marked in red in Fig. 10 are clearly subtidal, and can theoretically be considered marine limiting points, they were not used to build the curve as they do not maintain a direct relation with the MRMSL but rather represent different altitudes of the seabed. The MRMSL curve shows roughly three phases. During the first phase, between c. 7250 and 6500 cal. BP, the curve is steep with high rise rates (>1mm/yr.), and the Relative Sea-Level (RSL) jumps in some centuries from −6 to −2.3 m with respect to its current level. During this phase, the maximum geographical extension of the transgression is reached at the beginning of the 5th millennium cal. BC as shown by the lithostratigraphic data (Figs. 7-10). This very high rate of RSL rise suggests that during most of the Neolithic the landscape changes in this area, which document a quite flat and shallow coastal shelf profile (Perissoratis & Mitropoulos, 1989; Efstratiou, 2016), were very quick and dramatic. The marine transgression would certainly have been visible even in a single generation and could have forced societies to adapt quickly. Following this event, the potential Neolithic coastal sites in the study area were necessarily abandoned and inhabitants had to migrate gradually inland and/or uphill to avoid marine flooding. Such a rapid marine transgression episode may shed some light on the apparent absence of Neolithic occupation along this part of the Thracian coast. Indeed, the Lafrouda shell mound is the only recorded Neolithic coastal site in the region, and it lies partly underwater. This has led to the hypothesis that a number of Neolithic coastal sites between the 7th and mid-5th millennia BC may be underwater or buried by sediment (Ammerman et al., 2008; Efstratiou, 2016), as is the case in other coastal areas of the Mediterranean (e.g., Brisset et al., 2018; Berger, 2021). Our results are in line with this hypothesis: indeed, the discovery of pieces of fired clay at the top of Late Neolithic palaeosoils in two cores (AVZ1 and AVH7, Figs. 7 and 8), which represents an extremely limited sample, suggests that the density of Neolithic remains buried under lagoonal sediments could be relatively high in some areas around the Bouloustra promontory. If this is true, the quick fossilization of Neolithic remains and/or sites following rapid marine transgression would imply an excellent level of archaeological preservation in this coastal area.

The second section of the MRMSL curve (6500–2000 cal. BP) shows a marked slowdown of the rise rates, which are between 0.1 and 0.6 mm/yr. These rather moderated rates suggest that c. 4500 cal. BC the marine transgression was much slower and could partly have been compensated by sedimentary inputs from terrestrial areas. More stable coastal dynamics are also suggested by the formation of the first beach-barriers and lagoons in the area from c. 5000 cal. BC (Figs. 7-9). The dataset does not support a mid-Holocene high-stand in the area, although this hypothesis has already been widely discussed and contested for the Aegean (e.g. Brückner et al., 2010; Vacchi et al., 2014). By contrast, the MRMSL curve shows a relative slowdown in the rise of levels between 5500 and 3500 cal. BP, and especially in the 5th millennium cal. BP, with a MRMSL of −1.5 m with respect to the current level. Although a distortion due to the nature of the dataset and the process of construction of the curve cannot be totally discarded, this slowdown might instead represent a period of slight tectonic uplift of the Abdera horst, as other authors have already suggested (Pavlopoulos et al., 2012). It is noteworthy that this phase seems to correspond to a short emersion phase with incipient pedogenesis in the Valta Zambaki marsh (see Figs. 7 and 8) some centuries before 1450 cal. BC, which is indicative of a sedimentary accumulation rate exceeding the RSL rise in the lagoon. The impact of RSL variations documented between the second half of the Late Neolithic and the Late Bronze Age on local human populations is difficult to assess as archaeological data are very scarce. However, increased coastal stability (only a 1 m RSL rise in three millennia, between −2 and −1m) might have been an asset for settlement in the area. Our dataset suggests that when the Klazomenian colony was founded in c. 650 cal. BC (2600 cal. BP) the RSL was c. 70 cm lower than the present level (see Fig. 10), i.e., significantly higher than the rough estimation
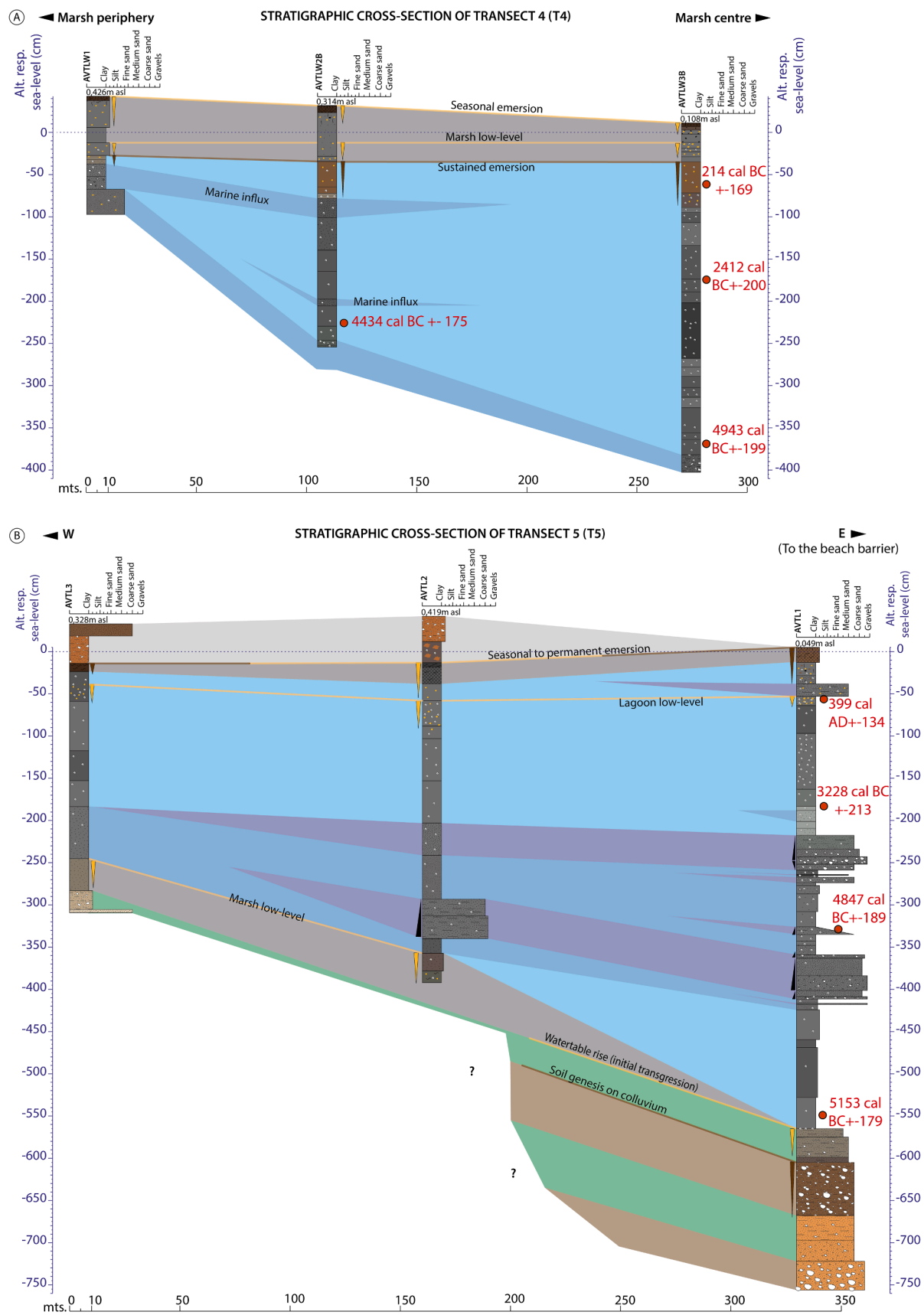
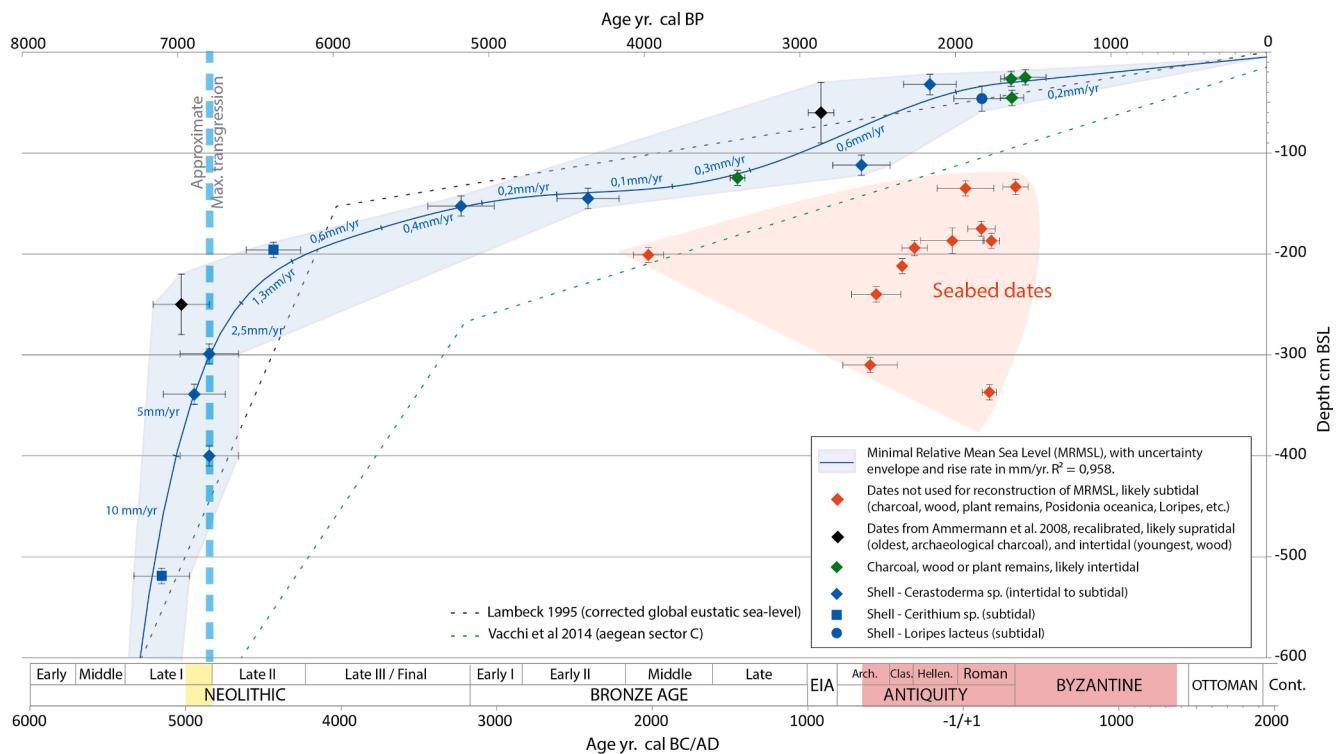**Fig. 9.** Stratigraphic cross-sections of Transects 4 and 5. The legend is the same than in Fig. 7.

Fig. 10. The MRMSL curve for the area of Abdera and Cape Bouloustra during the Middle and Late Holocene. Archaeological phasing from Kallintzi et al., 2001 and Glais, 2017. The periods with archaeological remains in the area are highlighted. Note that the X and Y axis are forced to 1950 (RSL −5 cm after Calafat & Gomis, 2009).

proposed by previous studies around Abdera (-1.2 to −1.5 m, Syrides & Psilovikos, 2004). The slight acceleration in the RSL rise during this period (and the third millennium BP in general) is not associated with any evident traces of marine invasion in the sedimentary record. Such a small transgressive event could have been compensated by increased sedimentary inputs into the coastal system after the foundation of the colony.

The last section of the MRMSL curve (2000 cal. BP onwards) is characterized by a rather slow and regular rise rate of 0.2 mm/yr., a relative slowdown respect precedent period. This rate appears consistent with other studies of changes in Mediterranean Sea-level suggesting that at c. 2000 cal. BP the RSL was quite close to today's (only −40 cm) and almost totally stabilized (e.g., Giaime et al., 2021). From this date onwards, we can assume that the very limited RSL rise was easily overwhelmed by sedimentary accretion and other coastal geomorphological dynamics related with shoreline progradation, as shown by our lithostratigraphic data and by many other studies in the Aegean and the Eastern Mediterranean as a whole (Vött et al., 2004; Kraft et al., 2007; Brückner et al., 2017; Giaime et al., 2022 i.a.). From an archaeological perspective, this assumption would mean that most structures from the Greek or Roman periods that were built at sea-level are likely to have been preserved underwater or buried at limited depths that are reachable by traditional or underwater excavations.

The general shape of our MRMSL curve is very similar to the corrected global eustatic sea-level curve during the Middle and Late Holocene (Lambeck & Purcell, 2005; Lambeck et al., 2014, see Fig. 10). The fact that this stretch of the Thracian coast constituted by the Abdera horst conforms to the general theoretical model, indicates that it has been subject to very few Holocene tectonic movements. By contrast, neighbouring areas such as Thasos and Samothrace are known to have significant subsiding and uplift trends respectively, which are clearly due to the interplay of active faults affecting both islands. Available RSL regional curves were known to be unreliable due to the paucity of data and the different tectonic trends of these locations (Pavlopoulos et al.,

2012; Vacchi et al., 2014; Seeliger et al., 2021). Our MRMSL curve, based in 16 ^{14}C-dated samples gathered around Cape Bouloustra, represents a significant step forward with respect to recent studies and fills a gap in scholarship of the Northern Aegean by providing a robust reference for Holocene RSL changes in the area.

5.2. Palaeogeographic evolution in the area of the ancient Abdera

5.2.1. The Early and Middle Neolithic (before 5000 BC)

The reconstruction of Holocene palaeogeographic evolution in the study area is shown in Fig. 11. By the beginning of the Middle Holocene (6.2 kyr. cal. BC), regional estimations suggest that the RSL was c. −15 m in the Mediterranean after a very sharp rise during the Early Holocene (Lambeck et al., 2014; Benjamin et al., 2017). During the 6th millennium cal. BC, the RSL continued to rise to c. −6/-4m below its current level (see Fig. 10). The shoreline of the Thracian coast was therefore located a few kms SE of its current position, as suggested by its low profile and modest bathymetry (Efstratiou, 2016). The palaeogeographic settings of the area around the promontory of Cape Bouloustra may have been radically different to the Late Holocene landscape, as the area was totally subaerial before 5000 cal. BC. The palaeotopography of this period is currently buried under several meters of water and sediment, and its tentative reconstruction is based on the morphology and orientation of the remaining terrestrial landforms, shallow reefs, and geological faults. The area was by then a hilly massif located a few kms from the sea, dissected by small valleys with thalwegs of several streams running in all directions, forming an almost radial pattern (Fig. 11A). A hypothetical NNW-SSE fault (IGME, 1980) may have controlled the main drainage axis in the western area of the massif. The results presented here point to a series of "dry" superficial deposits including alluvial and colluvial deposits, with different palaeosoils developed on pedo-sedimentary sequences responding to different cycles of wetter and dryer conditions (e.g., AVZ1 in Figs. 7 and 8, AVTL1 in Fig. 9). These sequences, which likely follow hypothetical palaeocatenas, hold

significant morpho-climatic and palaeoenvironmental information and may be valuable archives for future works focusing on Early Holocene and Early to Middle Neolithic occupation in the area (Figs. 7-9). The discovery of fragments of fired clay in cores AVH7 and AVZ1 (see previous section) probably indicates an extended presence of Late Neolithic (late 6th to early 5th millennium BC) occupations around the buried thalwegs of the W and NW flanks of the massif, which is consistent with the results obtained from prospections in the neighbouring hills (Georgiadis et al., 2022). With their fertile alluvial deposits and available freshwater, such areas were probably the most suitable places for farmers of the late 6th millennium BC.

5.2.2. From the Late Neolithic to the foundation of Abdera (5000 BC- 650 BC)

This landscape was submerged around 5000 cal. BC, when the rapid sea-level rise led the marine transgression to arrive at its maximum extent (see previous section), flooding all the lowlands around the Bouloustra massif (see Fig. 3). Inland beach-ridges preserved in the area of Tuzla Gyol (see Fig. 6 n°0, and Fig. 11B) indicate that the coastal promontory then became a peninsula which was only connected to the mainland at the north by a narrow "neck" at c. 5 m a.s.l., as suggested by previous studies (Syrides & Psilovikos, 2004). However, our work shows that this peculiar geographic configuration was extremely short-lived: following the litho-stratigraphic data (see Figs. 7-9) extensive beach-barrier systems with closed lagoons and marshy areas seem to have developed quickly after 5000 cal. BC in the areas of Tuzla Gyol and Valta Zambaki (see Figs. 3 and 11B). By then the first area already had a shoreline that was very similar to that of the present-day, whereas the situation in the western side of the cape consisted of a deep embayment with the shoreline lying almost 2 km inland with respect to where it is now. The rest of the shoreline in the area developed a rocky coast morphology with very limited beaches and cliffs on gneiss and reefs, some of which are now buried or landlocked (Figs. 6 and 11B). A small islet, presumably connected to the mainland by a sandbar or a shoal forming a tombolo, existed on the W side of the promontory. These palaeogeographic and environmental settings remained roughly stable between 5000 and 650 cal. BC. The sea-level continued to rise gradually (Fig. 10), and the sediment accumulation rate in the lagoons decreased progressively, although both sides of the colony present a slightly different evolution. Washover episodes due to HEE were more frequent in the Tuzla Gyol area in the 5th and 4th millennia BC, whereas closed lagoonal conditions seem more consolidated for the same period in the Valta Zambaki lagoon. In the latter, the recurrence of low-stand and/or short emersion episodes suggest that the sedimentary infilling of the basin occurred at a very similar (or occasionally faster) pace to that of the sea-level rise, and that the water depth was almost always shallow during the life-cycle of the lagoon.

5.2.3. The Greek and Roman periods (650 BC − 400 AD)

The palaeogeographic conditions were not very different at c. 650 cal. BC, when the Klazomenians founded the Archaic colony. On the eastern side of Cape Bouloustra, the lagoon of Tuzla Gyol was slowly silting up. On the NW side, the Valta Zambaki lagoon had significantly shallowed and was almost a marsh with its peripheral areas emerged (Fig. 11C). The colonists built a ship shed directly on the beach at the NW extremity of the city wall, which was surely accompanied by other harbour facilities on the western bay (Moustaka et al., 2004). During the subsequent 350 years landscape changes were minor, and the lagoons and other wetlands continued to infill slowly. By the middle of the 4th c. BC, the city moved southwards to a new *enceinte* (Moustaka et al., 2004; Kallintzi, 2011, see Fig. 3). Previous studies have suggested that the coastline could already have started to prograde significantly in this period due to the silting up of the bay (Syrides & Psilovikos, 2004). However, our results show that the water depth at almost the head of the bay (AVH1 and AVH2, Fig. 7) was approx. 1.75 m in this period, and that the coastline was in a very similar position to where it was in the

previous millennia. The silting up of the bay, if it had started, could only have been very incipient, suggesting that the movement of the city in the mid-4th c. BC was not due to this reason, but rather to other factors such as major defeats against the Thracians and the sacking of the city in 376–375 BC, or the conquest by the Macedonians in 353–346 BC. This historical narrative for Abdera, supported by our results, differs from the paradigm of the "race to the sea" depicted by many geoarchaeological studies of ancient port cities in the Aegean and the Mediterranean (e.g., Brückner et al., 2005; Morhange et al., 2011; Giaime et al., 2019 i.a.).

Coastal progradation and the silting up of the bay became more evident after 300 cal. BC (Fig. 11D), although our palaeogeographic reconstruction shows that these phenomena were weaker and much less extended than suggested by previous research (Syrides & Psilovikos, 2004). The accretion and thickening of the beach-barrier reached several hundred meters (500–800 m, Figs. 7 and 11D). Despite this change, our data suggest there was still an inlet of partially open water (or an open lagoon) immediately in front of the western side of the city, perhaps functioning as an outlet for the Valta Zambaki marsh.

The cause behind the silting up of the bay and the coastal progradation, which continued in the following centuries, is crucial to forming an understanding of the socio-environmental interaction around Abdera. The results obtained in this study rule out changes in tectonics and/or sea-level as the major drivers of shoreline change during the Greek period (see section 5.1). Previous studies have suggested that silting could mainly be due to an increased sediment input by the river Nestos, or to an avulsion bringing a channel directly to the harbour of the colony, although the possible influence of the economic activities of the colonists on the sedimentary budget has also been raised (see Kallintzi, 2011). Our litho-stratigraphic transects show no evidence of a channel running off the Nestos into the bay of Abdera in this period but instead show a total absence of alluvial sediments in the bay (see Figs. 7-9). Moreover, the shape, size, and position of the massive sand bodies 2–3 and 4–6 (Figs. 5 and 6) which silted up the harbour from 300 cal. BC onwards, clearly indicate that at this time the mouth of the Nestos was located at least 5–7 km, or even more, west of Abdera. Indeed, many ancient channels of the river are visible on the eastern side of the Nestos delta in aerial pictures taken in 1938 and 1945 and in satellite imagery (Fig. 5), which suggests that active channels of the river were functional in that area in undetermined periods of the last few centuries, perhaps even millennia. A direct avulsion into the bay can thus be discarded and any sediment from the mouth of the Nestos potentially contributing to any silting processes was necessarily reworked, redistributed, and brought from the W or SW by coastal currents over several km.

Interestingly, the main winds and currents in the area (including the coastal drift) move in exactly the opposite direction (from the NE and parallel to the coast, see Kourafalou & Barbopoulos, 2003; Xeidakis et al., 2010; Kokkos et al., 2021), and the embayment is very well protected from winds and sedimentation by Cape Bouloustra (Fig. 1). Besides this, in most meteorological situations the Nestos sedimentary plume is driven westwards by these currents through the Thasos strait to the Kavala Gulf (Kamidis et al., 2011, 2015; Sylaios et al., 2013, see Fig. 1). These peculiar settings are undoubtedly the main reason for the remarkable stability of the shoreline in the bay of Abdera between 5000 and 300 cal. BC. Therefore, natural geomorphological changes can hardly be invoked to explain the sudden silting up of the bay. Additionally, hydro-climatic conditions are broadly stable during the middle of the first millennium BC in the Eastern Mediterranean, and despite the possibility that drier conditions may have locally occurred they still would not have been likely enough to cause unprecedented changes in sedimentary budgets (Psomiadis et al., 2018; Finné et al., 2019). The silting up of the bay may instead be related to the only differential event in the area from 5000 cal. BC onwards which had the potential to cause major forcing of sedimentary and geomorphic equilibrium: the foundation of Abdera in 654 BC.

The development of the productive activities of the colony in the following centuries is documented in the archaeological record both in
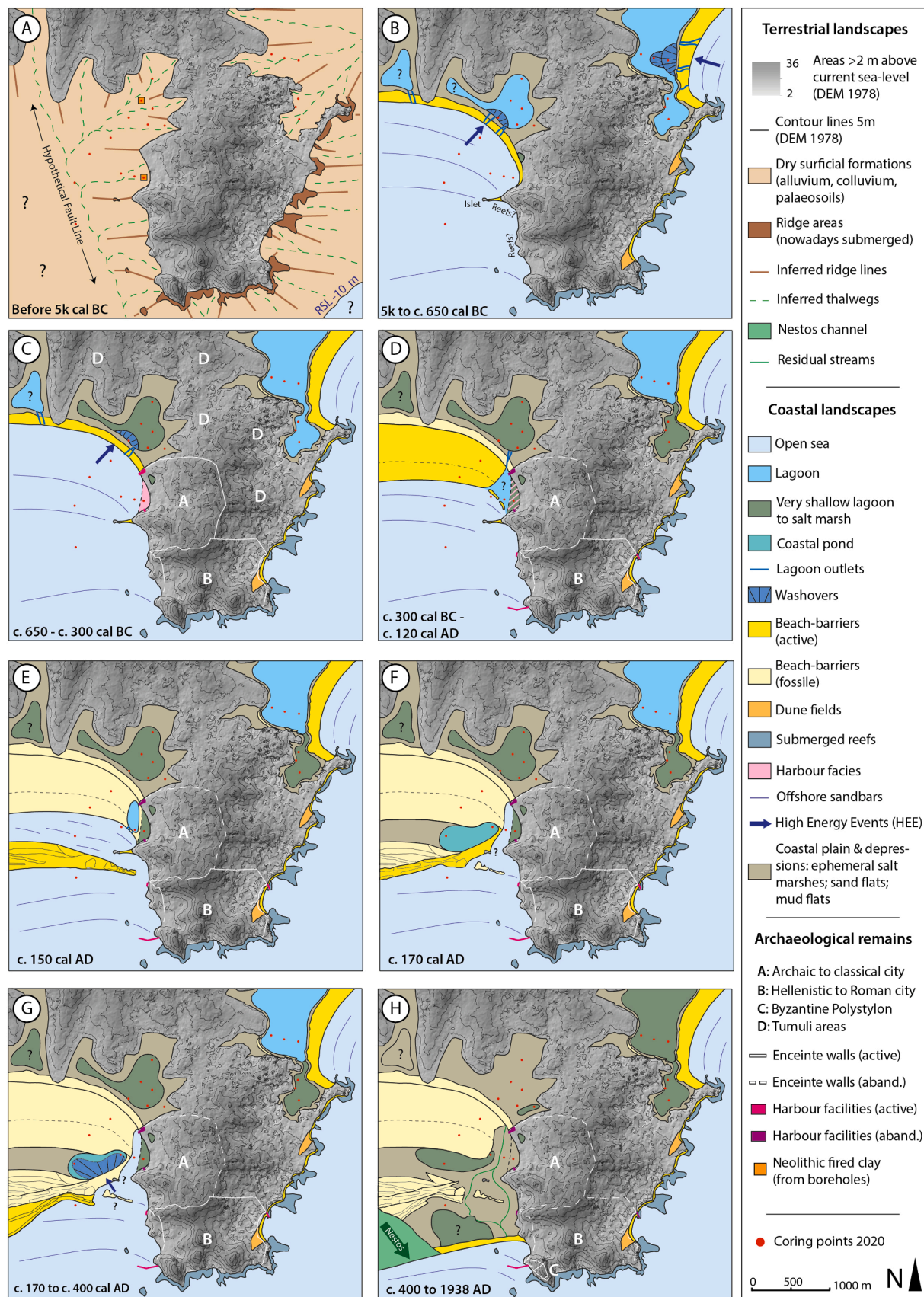
Fig. 11. Palaeogeographic evolution in the area of ancient Abdera between the Early Holocene and 1938 AD.

the urban area itself and its surrounding territory (Kallintzi, 2011; Kallintzi et al. 2021). Increased agricultural activities, with the expansion of farmsteads in the 5th and 4th c. BC (Georgiadis et al., 2022), could have caused significant soil erosion and extra inputs into the coastal sedimentary system at local and micro-regional scales. Mining and quarrying activities in the Rhodope mountains, which host abundant marble plus silver, gold, and iron ores, were certainly developed by the Thracians to trade with the Abderitans and the Thasians (Nerantzis, 2015; Kallintzi et al., 2021). The exploitation of such mineral resources may also have caused significant increases of soil erosion at a regional scale and boosted the Nestos sedimentary load. Similar anthropogenic forcings of hydro-sedimentary systems have been detected from the 4th and 3rd centuries BC in the Thracian region, due to major changes in land-use (Lespez, 2003; Glais et al., 2016). At Abdera, increased sedimentary inputs into the coastal system started from 300 cal. BC to thicken the beach-barrier in front of the Valta Zambaki marsh. This led to the gradual silting up of the bay and shoreline progradation. Despite this change in coastal dynamics, most of the bay remained navigable until c. 100–120 cal. AD (Fig. 11D).

By c. 150 cal. AD, a large sandbar (n°4 in Fig. 6) of several kms in length (see Fig. 5) had formed in the middle of the bay of Abdera (Fig. 11E). This sandbar could initially have developed offshore due to the persistent increased supply of sediments to the coastal system. It would then have migrated shorewards as previous studies have suggested (Syrides & Psilovikos, 2004), although our data situates the formation of this barrier several centuries later than they have proposed. This sandbar was not completely closed and the back-barrier area was well connected with the sea (Fig. 11E). Its location did not significantly disturb access to the sea from the harbour facilities of the Hellenistic and Roman city. At the same time, coastal accretion had also progressed slightly and the inlet in front of the Archaic-Classical city was now a small, relatively open lagoon (see base of AVH3 in Fig. 8A).

Circa 170 cal. AD, the sand barrier had partly collapsed, and a new one with an oblique direction (n°5 in Fig. 6) had welded its remains to the previous beach-barrier systems. This new beach-barrier closed the back-barrier space westwards, isolating a small coastal pond within the sandflats and mudflats (see AVH6 and AVH4 in Fig. 8A, and Fig. 11F). By contrast, the small lagoon in front of the Archaic-Classical city was re-opened and became a narrow sea inlet or channel, perhaps connected to the outlet of the Valta Zambaki marsh. This configuration prevailed with few changes until c. 400 cal. AD (Fig. 11G). The active beach-barrier continued to thicken with a new sandbar (n° 6 in Fig. 6), while the small inlet was being quickly infilled. Despite the city still having good access to the sea, Abdera started to decline during the 2nd-3rd centuries AD and was almost abandoned by the middle of the 4th c. AD, likely due to enemy incursions and to the shift of the economical axis from the coast to the *Via Egnatia* at the feet of the Rhodope mountains (Kallintzi, 2011, 2018).

5.2.4. From Late Antiquity to the modern era (400 AD onwards)

In the centuries following 400 cal. AD, a major HEE affected the shore to the West of the colony, extending across hundreds of meters and penetrating 2 km inland (see Figs. 7 and 12). It draped a considerable area with sandy materials (Fig. 12) and carried extremely coarse and unsorted materials of marine origin including broken shells or extremely rounded ceramics to several points. Additionally, fragments of beach-rock, rip-up clasts and floating woody debris are evidence of the very high hydrodynamic power of the flow and backflow (see Figs. 7-9 and 12). Taken together, all this evidence indicates that the HEE that left these deposits was clearly a tsunami that hit the area in Late Antiquity.

Following the distribution of these deposits, the wave would have impacted the coast at both sides of the promontory of Cape Bouloustra (Fig. 12A). The eastern areas (the Tuzla Gyol lagoon), which had a thick and likely robust sandbar developed from 5000 cal. BC and were partly sheltered by the shape of the coast, suffered only a minor washover. Impacts on the western side were much more significant: the

tsunamigenic waves entered the bay and probably overtopped or breached the small pond of AVH4 and AVH6. In their progression northwards they entered the narrow inlet just in front of the Archaic harbour area (see Figs. 11 and 12), where they likely grew in size and accelerated due to the Venturi effect (e.g., Cardenas-Jiron, 2013), thus increasing their destructive power. The hydrodynamic energy of the waves was then likely enough to cross the sandbar separating the inlet from the Valta Zambaki marsh, where they formed a very large washover fan covering the entire area.

Although the washover deposits caused by this tsunami may have been slightly erosive in our sequences, the available radiocarbon dates allow us to reasonably assume that the event occurred during the 5th c. AD, or slightly later. Previous research has found robust evidence of a tsunami in Late Antiquity in several locations on the Thracian coast East of Abdera ("Event Z" in Mathes-Schmidt et al., 2013, see Fig. 12). The dates they mention were obtained directly from the tsunamigenic layers and after recalibration with MARINE20 curve for homogeneity, they show that a tsunami hit the coast around 600 ± 150 cal. AD. Interestingly, there is historical evidence of a tsunami in 544 AD on the coast of Aegean Thrace: a regional earthquake that originated in the Black Sea may have caused marine slumps triggering tsunamis in the Northern Aegean (Papadopoulos et al., 2011, 2014). Considering that the Thracian coast is one of the less tsunamigenic areas in the Aegean, with infrequent big tsunamis (Papadopoulos & Fokaefs, 2005; Papadopoulos et al., 2014), and that only a single tsunami layer has been found for Late Antiquity in the sedimentary sequences retrieved at Abdera and other locations on the Thracian coast (Mathes-Schmidt et al., 2013), all this evidence clearly corresponds to a single tsunami that can be dated to 544 cal. AD.

This tsunami undoubtedly had a significant morphogenic effect upon the bay of Abdera: it brought massive amounts of sediment to the coastal lowlands and contributed to the acceleration of the silting process of the bay and coastal progradation, leading to major palaeogeographic and palaeoenvironmental changes in the area in the subsequent centuries. Besides flooding the wetlands and sandy lowlands without any great productive value, the wave certainly destroyed or buried all of the remaining sea-related infrastructures, such as the Archaic-Classical harbour. However, the real impact of this catastrophic event for Abdera was probably limited as the city had been abandoned a few centuries earlier.

Despite the lack of radiocarbon data, the location of the Byzantine harbour, which was active at least until the 14th c., indicates that during the Middle Ages progradation of the coast was significant and reached a very similar position to the present day (Fig. 11H), suggesting the persistence of anthropogenic forcing of sedimentary budgets. A new sandbar developed and formed a beach-barrier c. 500 m south of the previous one, disconnecting large back-barrier areas from the sea. The latter became sand flats, mud flats, or marshes which were locked between the different generations of beach-barriers. Lagoons and wetlands surrounding the promontory became marshy or almost dry sandflats and mudflats (Fig. 11H). In a posterior phase, likely occurring during the 19th or the early 20th c. an avulsion channel of the Nestos cut across all the previous sedimentary deposits in the bay, including the medieval beach-barrier.

6. Conclusions

Based on the radiocarbon data from the cores, the first detailed and accurate Holocene sea-level curve for this sector of the Northern Aegean has been built and presented in this article. This curve is consistent with global eustatic models, thus confirming that the Abdera horst was subject to few tectonic movements during the Holocene. The palaeogeographic evolution of the area around Abdera from the Mid-Holocene onwards was reconstructed here, with the main processes and phases of landscape change and their potential drivers also identified.

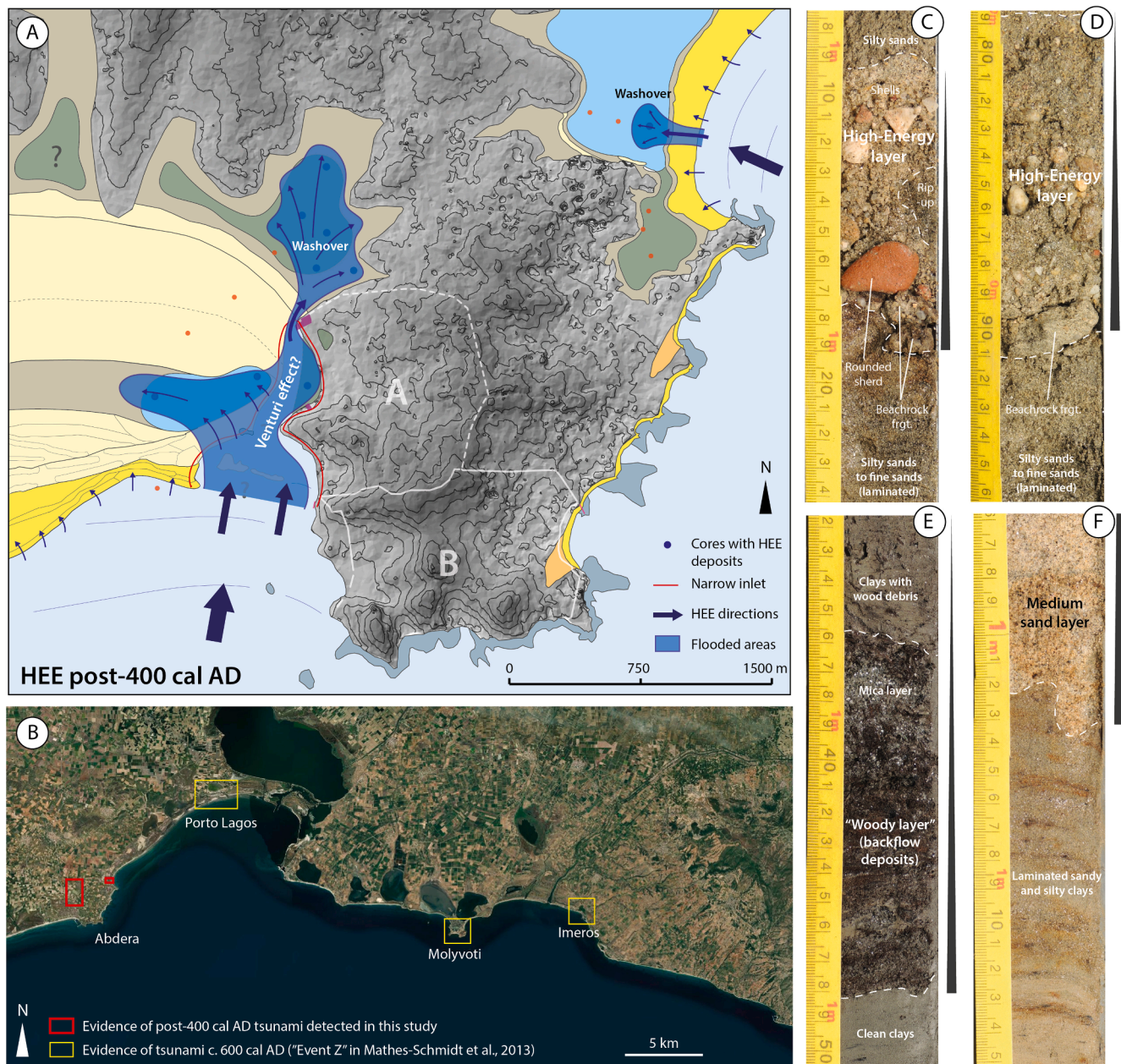Before 5000 cal. BC, the area was terrestrial due to a much lower sea-

Fig. 12. A) Distribution of the points with post-400 AD tsunami deposits and reconstruction of the areas flooded by the event; B) Location of the evidence for tsunamis in Late Antiquity on the Thracian coast to the east of Abdera; C-F: selection of different facies interpreted as tsunami deposits (C & D: AVH7 (twin cores); E: AVH4; F: AVZ1).

level. The first evidence for the drowned Early and Middle Holocene landscapes of this coastal region that was likely occupied with a certain density by Late Neolithic societies was found. This discovery holds significant archaeological potential for the remains buried below the coastal sediments. The Mid-Holocene transgression peaked in the area at c. 5000 cal. BC. The Bouloustra promontory almost became a peninsula surrounded by beach-barriers and lagoons, after which the landscape remained roughly stable for several millennia.

In the 7th and 6th c. BC, the Klazomenians followed by the Teians founded and settled at Abdera on the west side of the promontory, where a large bay provided an excellent harbour area as shown by our cores. The results presented here suggest that the displacement of the city to a new *enceinte* one km southwards in the mid-4th c. BC was not due to the silting up of the bay and the harbour, as such processes were by then very incipient, but was rather caused by historical events.

The process of coastal progradation intensified substantially after

300 cal. BC. Given the steady tectonic and climatic context during this period, it is hypothesized here that the development of Abdera likely caused a significant rise in anthropogenic soil erosion at local and microregional scales, thereby increasing sedimentary inputs to the coastal system. After several centuries, these processes might have culminated in a general forcing of the sedimentary system, leading to the gradual silting up of the bay and a marked coastal progradation from 300 cal. BC onwards, although draught remained enough for navigation in most of the bay until c. 120 cal. AD. By the mid-2nd c. AD these dynamics accelerated and the coastline advanced hundreds of metres southwards, followed by a more gradual progradation in the subsequent centuries. During this period Abdera began to decline and was finally abandoned after the mid-4th c. AD, despite still having fully functional harbours. Our results support the idea that this demise was not caused by changes to the coastal landscapes, but through a more Braudelian perspective by the long-term trend to a shift of the economical axis from the sea to the

roman road at the feet of the Rhodope mountains.

After c. 400 cal. AD a tsunami hit the coastal lowlands west of Abdera, reaching up to 2 km inland and certainly causing major geomorphic effects. The convergence of our radiocarbon dates with those previous studies have taken from this sector of the Thracian coast and historical data suggest that this tsunami occurred in 544 cal. AD. After this catastrophic event, the coast continued to prograde further south during the Byzantine period reaching a position similar to where it currently lies.

Beyond its regional relevance in the Northern Aegean, this study represents an outstanding example of the key role an integrated geoarchaeological approach can play in discussions of causality in complex and non-linear socio-environmental interactions and their contribution to long-term landscape evolution in coastal areas, especially by helping to challenge historical narratives and overcome deterministic visions and catastrophism. Finally, the rich sedimentary records retrieved around Abdera also hold significant potential for further research: forthcoming high-resolution and multi-proxy palaeoenvironmental and geoarchaeological analysis will provide a finer, much more comprehensive, and nuanced picture of the history of the city and its environment from the Neolithic until the present day.

Declaration of Competing Interest

The authors declare that they have no known competing financial interests or personal relationships that could have appeared to influence the work reported in this paper.

Data availability

Data will be made available on request.

Acknowledgements

References

Abadie, A., Pace, M., Gobert, S., Borg, J.A., 2018. Seascape ecology in Posidonia oceanica seagrass meadows: Linking structure and ecological processes for management. Ecol. Ind. 87, 1–13.

Amato, V., Cicala, L., Valente, E., Ruello, M.R., Esposito, N., Ermolli, E.R., 2021. Anthropogenic amplification of geomorphic processes along the Mediterranean coasts: A case-study from the Graeco-Roman town of Elea-Velia (Campania, Italy). Geomorphology 383.

Ammerman, A., Efstratiou, N., Ntinou, M., Pavlopoulos, K., Gabrielli, R., Thomas, K., Mannino, M., 2008. Finding the early Neolithic in Aegean Thrace: The use of cores. Antiquity 82 (315), 139–150.

Anacleto, P., Maulvault, A.L., Barbosa, V., Nunes, M.L., Marques, A., 2016. Shellfish: Characteristics of Crustaceans and Mollusks. Encyclopedia of Food and Health, (1st ed.). Elsevier Ltd.

Arche, A. (2010). Sedimentología. Del proceso físico a la cuenca sedimentaria. Madrid: CSIC.

Bellanova, P., Frenken, M., Nishimura, Y., Schwarzbauer, J., Reicherter, K., 2021. Tracing woody-organic tsunami deposits of the 2011 Tohoku-oki event in Misawa (Japan). Sci. Rep. 11, 8947.

Benjamin, J., Rovere, A., Fontana, A., Furlani, S., Vacchi, M., Inglis, R.H., Galili, E., Antonioli, F., Sivan, D., Miko, S., Mourtzas, N., Felja, I., Meredith-Williams, M., Goodman-Tchernov, B., Kolaiti, E., Anzidei, M., Gehrels, R., 2017. Late Quaternary sea-level changes and early human societies in the central and eastern Mediterranean Basin: An interdisciplinary review. Quat. Int. 449, 29–57.

Berger, J. F. (2021). Geoarchaeological and Paleo - Hydrological Overview of the Central - Western Mediterranean Early Neolithic Human – Environment Interactions. Open Archaeology, 1371–1397.

Blondel, J., 2006. The ' Design ' of Mediterranean Landscapes : A Millennial Story of Humans and Ecological Systems during the Historic Period. Hum. Ecol. 34, 713–729.

Brisset, E., Burjachs, F., Ballesteros Navarro, B.J., Fernández-López de Pablo, J., 2018. Socio-ecological adaptation to Early-Holocene sea-level rise in the western Mediterranean. Global Planet. Change 169, 156–167.

Brückner, H., Vött, A., Schriever, A., Handl, M., 2005. Holocene delta progradation in the eastern Mediterranean– case studies in their historical context. Méditerranée 95–106.

Brückner, H., Kelterbaum, D., Marunchak, O., Porotov, A., Vött, A., 2010. The Holocene sea level story since 7500 BP - Lessons from the Eastern Mediterranean, the Black and the Azov Seas. Quat. Int. 225 (2), 160–179.

Brückner, H., Urz, R., Seeliger, M., 2013. Geomorphological and geoarchaeological evidence for considerable landscape changes at the coasts of western Turkey during the Holocene. GeoRS Geopedology and Landscape Development Research Series 01, 81–104.

Brückner, H., Herda, A., Kerschner, M., Müllenhoff, M., Stock, F., 2017. Life cycle of estuarine islands — From the formation to the landlocking of former islands in the environs of Miletos and Ephesos in western Asia Minor (Turkey). J. Archaeol. Sci. Rep. 12, 876–894.

Butzer, K.W., 1982. Archaeology as Human Ecology: Method and Theory for a Contextual Approach. Cambridge University Press, Cambridge.

Butzer, K.W., 2005. Environmental history in the Mediterranean world: Cross-disciplinary investigation of cause-and-effect for degradation and soil erosion. J. Archaeol. Sci. 32 (12), 1773–1800.

Calafat, F.M., Gomis, D., 2009. Reconstruction of Mediterranean sea level fields for the period 1945–2000. Global Planet. Change 66 (3-4), 225–234.

Cañellas-Boltà, N., Riera-Mora, S., Orengo, H.A., Livarda, A., Knappett, C., 2018. Human management and landscape changes at Palaikastro (Eastern Crete) from the Late Neolithic to the Early Minoan period. Quat. Sci. Rev. 183, 59–75.

Cardenas-Jiron, L.A., 2013. The Chilean earthquake and tsunami 2010: a multidisciplinary study of Mw8. 8. WIT Press, Maule.

Cramer, W., Guiot, J., Fader, M., Garrabou, J., Gattuso, J.-P., Iglesias, A., Lange, M.A., Lionello, P., Llasat, M.C., Paz, S., Peñuelas, J., Snoussi, M., Toreti, A., Tsimplis, M.N., Xoplaki, E., 2018. Climate change and interconnected risks to sustainable development in the Mediterranean. Nat. Clim. Chang. 8 (11), 972–980.

Davidson-Arnott, R., 2010. Introduction to Coastal Processes and Geomorphology. Cambridge University Press, Cambridge.

Davis, R.A., Yale, K.E., Pekala, J.M., Hamilton, M.V., 2003. Barrier island stratigraphy and Holocene history of west-central Florida. Mar. Geol. 200 (1-4), 103–123.

De Martini, P.M., Bruins, H.J., Feist, L., Goodman-Tchernov, B.N., Hadler, H., Lario, J., Mastronuzzi, G., Obrocki, L., Pantosti, D., Paris, R., Reicherter, K., Smedile, A., Vött, A., 2021. The Mediterranean Sea and the Gulf of Cadiz as a natural laboratory for paleotsunami research: Recent advancements. Earth Sci. Rev. 216, 103578.

Dearing, J.A., Acma, B., Bub, S., Chambers, F.M., Chen, X., Cooper, J., Crook, D., Dong, X.H., Dotterweich, M., Edwards, M.E., Foster, T.H., Gaillard, M.-J., Galop, D., Gell, P., Gil, A., Jeffers, E., Jones, R.T., Anupama, K., Langdon, P.G., Marchant, R., Mazier, F., McLean, C.E., Nunes, L.H., Sukumar, R., Suryaprakash, I., Umer, M., Yang, X.D., Wang, R., Zhang, K., 2015. Social-ecological systems in the Anthropocene: The need for integrating social and biophysical records at regional scales. Anthropocene Review 2 (3), 220–246.

Devillers, B., Bony, G., Degeai, J.-P., Gascò, J., Lachenal, T., Bruneton, H., Yung, F., Oueslati, H., Thierry, A., 2019. Holocene coastal environmental changes and human occupation of the lower Hérault River, southern France. Quat. Sci. Rev. 222, 105912.

Efstratiou, N. (2016). Archaeological visibility and early farming habitation patterns in coastal Thrace (Greece) – an overview . Southeast Europe and Anatolia in prehistory. Essays in honor of Vassil Nikolov on his 65th anniversary, 105–115.

Ejarque, A., Julià, R., Reed, J.M., Mesquita-Joanes, F., Marco-Barba, J., Riera, S., Dias, J. M., 2016. Coastal evolution in a mediterranean microtidal zone: Mid to late holocene natural dynamics and human management of the castelló lagoon, NE Spain. PLoS One 11 (5), e0155446.

Engel, M., Brückner, H., 2011. The identification of palaeo-tsunami deposits – a major challenge in coastal sedimentary research The era of overlooking and misinterpretation. Coastline Reports 17, 65–80.

Engel, M., Pilarczyk, J., Matthias May, S., Brill, D., Garrett, E., 2020. Geological Records of Tsunamis and Other Extreme waves. Elsevier.

Finné, M., Woodbridge, J., Labuhn, I., Roberts, C.N., 2019. Holocene hydro-climatic variability in the Mediterranean: A synthetic multi-proxy reconstruction. Holocene 29 (5), 847–863.

Florenzano, A., Zerboni, A., Carter, J.C., Clò, E., Mariani, G.S., Mercuri, A.M., 2022. Environmental and land use changes in a Mediterranean landscape: Palynology and geoarchaeology at ancient Metapontum (Pantanello. Quat. Int. 635, 105–124.

Fruergaard, M., Andersen, T.J., Nielsen, L.H., Johannessen, P.N., Aagaard, T., Pejrup, M., 2015. High-resolution reconstruction of a coastal barrier system: Impact of Holocene sea-level change. Sedimentology 62 (3), 928–969.

Georgiadis, M., Kallintzi, C., Garcia-Molsosa, A., Orengo, H.A., Kefalidou, E., Motsiou, P., 2022. The Archaeological Survey at Abdera and Xanthi 2015–2019: Long-term analysis of colonial relations in Thrace. Archaeol. Anthropol. Sci. 14 (9).

Giaime, M., Marriner, N., Morhange, C., 2019. Evolution of ancient harbours in deltaic contexts: A geoarchaeological typology. Earth Sci. Rev. 191, 141–167.

Giaime, M., Jol, H.M., Salmon, Y., López, G.I., Hamid, A.A., Bergevin, L., Bauman, P., McClymont, A., Sailer-Haugland, E., Artzy, M., 2021. Using a multi-proxy approach to locate the elusive Phoenician/Persian anchorage of Tel Akko (Israel). Quat. Int. 602, 66–81.

Giaime, M., Artzy, M., Jol, H.M., Salmon, Y., López, G.I., Abu Hamid, A., 2022. Refining Late-Holocene environmental changes of the Akko coastal plain and its impacts on the settlement and anchorage patterns of Tel Akko (Israel). Mar. Geol. 447.

Glais, A., 2017. Interactions Sociétés-Environnement en Macédoine orientale (Grèce du Nord) depuis le début de l'Holocène: Approche multiscalaire et paléoenvironnementale. Normandie Université.

Glais, A., Lespez, L., Davidson, R., López-Sáez, J.A., Birée, L., 2016. 3000 ans de détritisme en Grèce du Nord: entre fluctuations climatiques et anthropisation des zones humides. Géomorphologie: relief, processus, environnement 22 (2), 187–208.

González-Villanueva, R., Pérez-Arlucea, M., Costas, S., Bao, R., Otero, X.L., Goble, R., 2015. 8000 years of environmental evolution of barrier–lagoon systems emplaced in coastal embayments (NW Iberia). Holocene 25, 1786–1801.

Goslin, J., Clemmensen, L.B., 2017. Proxy records of Holocene storm events in coastal barrier systems: Storm-wave induced markers. Quat. Sci. Rev. 174, 80–119.

Heaton, T.J., Köhler, P., Butzin, M., Bard, E., Reimer, R.W., Austin, W.E.N., Bronk Ramsey, C., Grootes, P.M., Hughen, K.A., Kromer, B., Reimer, P.J., Adkins, J., Burke, A., Cook, M.S., Olsen, J., Skinner, L.C., 2020. Marine20 - The Marine Radiocarbon Age Calibration Curve (0–55,000 cal. BP). Radiocarbon 62 (4), 779–820.

IGME. (1980). Geological Map of Greece 1:50.000 - Sheet n° 48 Avdhira-Mesi.

Kallintzi, C., 2011. The chora of Abdera: a contribution to the archaeology and historical topography of the south region of the prefecture of Xanthi. University of Thessaly.

Kallintzi, C., 2018. The Roman city of Abdera and its territory. Bulletin of the National Archaeological Institute 44, 21–30.

Kallintzi, C., Terzopoulou, D., Zekos, N., Dadaki, S., 2001. Abdera Polystylon - Archaeological guide, Athens.

Kallintzi, C., Georgiadis, M., Kefalidou, E., Xydopoulos, I., 2021. Greeks and Thracians at Abdera and the Xanthi- Nestos Area in Aegean Thrace. In: Driessen, J., Vanzetti, A. (Eds.), Communication Uneven. Acceptance of and Resistance to Foreign Influences in the Connected Ancient Mediterranean. Louvain-la-Neuve: Collection Aegis. Presses Universitaires de Louvain.

Kamidis, N., Sylaios, G., Tsihrintzis, V.A., 2011. Modeling the Nestos River plume dynamics using ELCOM. Desalin. Water Treat. 33 (1-3), 22–35.

Kamidis, N., Sylaios, G., Tsihrintzis, V.A., 2015. Nestos River plume dynamics under variable physical forcing. Πανελλήνια και Διεθνή Γεωγραφικά Συνέδρια, Συλλογή Πρακτικών, pp. 549–566.

Kaniewski, D., Van Campo, E., Morhange, C., Guiot, J., Zviely, D., Shaked, I., Otto, T., Artzy, M., 2013. Early urban impact on Mediterranean coastal environments. Sci. Rep. 3, 1–5.

Kokkos, N., Zoidou, M., Zachopoulos, K., Nezhad, M.M., Garcia, D.A., Sylaios, G., 2021. Wind climate and wind power resource assessment based on gridded scatterometer data: A thracian sea case study. Energies 14, 1–16.

Koukousioura, O., Kouli, K., Vouvalidis, K., Aidona, E., Karadimou, G., Syrides, G., 2020. A multi-proxy approach for reconstructing environmental dynamics since the mid Holocene in Lake Ismarida (Thrace, N. Greece). Rev. Micropaleontol. 68.

Kourafalou, V.H., Barbopoulos, K., 2003. High resolution simulations on the North Aegean Sea seasonal circulation. Ann. Geophys. 21, 251–265.

Koutsoubas, D., Arvanitidis, C., Dounas, C., Drummond, L., 2000. Community structure and dynamics of the Molluscan Fauna in a Mediterranean lagoon (Gialova lagoon, SW Greece). Belg. J. Zool. 130, 131–138.

Kraft, J.C., Bückner, H., Kayan, I., Engelmann, H., 2007. The geographies of ancient Ephesus and the Artemision in Anatolia. Geoarchaeology 22 (1), 121–149.

Lambeck, K., Purcell, A., 2005. Sea-level change in the Mediterranean Sea since the LGM: Model predictions for tectonically stable areas. Quat. Sci. Rev. 24 (18-19), 1969–1988.

Lambeck, K., Rouby, H., Purcell, A., Sun, Y., Sambridge, M., 2014. Sea level and global ice volumes from the Last Glacial Maximum to the Holocene. PNAS 111 (43), 15296–15303.

Lespez, L., 2003. Geomorphic responses to long-term land use changes in Eastern Macedonia (Greece). Catena 51 (3–4), 181–208.

Lespez, L., Lescure, S., Saulnier-Copard, S., Glais, A., Berger, J.F., Lavigne, F., Pearson, C., Virmoux, C., Müller Celka, S., Pomadère, M., 2021. Discovery of a tsunami deposit from the Bronze Age Santorini eruption at Malia (Crete): impact, chronology, extension. Sci. Rep. 11, 1–15.

Malek, Ž., Verburg, P.H., R Geijzendorffer, I., Bondeau, A., Cramer, W., 2018. Global change effects on land management in the Mediterranean region. Glob. Environ. Chang. 50, 238–254.

Marriner, N., Morhange, C., 2006. The "Ancient Harbour Parasequence": Anthropogenic forcing of the stratigraphic highstand record. Sed. Geol. 186 (1-2), 13–17.

Marriner, N., Morhange, C., 2007. Geoscience of ancient Mediterranean harbours. Earth Sci. Rev. 80 (3-4), 137–194.

Marriner, N., Morhange, C., Kaniewski, D., Carayon, N., 2014. Ancient harbour infrastructure in the Levant: Tracking the birth and rise of new forms of anthropogenic pressure. Sci. Rep. 4, 1–11.

Mathes-Schmidt, M., Schwarzbauer, J., Papanikolaou, I., Syberberg, F., Thiele, A., Wittkopp, F., Reicherter, K., 2013. Geochemical and microfaunistical

investigations of tsunamigenic layers along the Thracian Coast (Northern Aegean Sea, Greece). Z. Geomorphol. 57 (4), 5–27.

Mayoral, A., Toumazet, J.-P., Simon, F.-X., Vautier, F., Peiry, J.-L., 2017. The highest gradient model: A new method for analytical assessment of the efficiency of lidar-derived visualization techniques for landform detection and mapping. Remote Sens. (Basel) 9 (2), 120.

Morhange, C., Blanc, F., Schmitt-Mercury, S., Bourcier, M., Carbonel, P., Oberlin, C., Prone, A., Vivent, D., Hesnard, A., 2003. Stratigraphy of late-Holocene deposits of the ancient harbour of Marseilles, southern France. Holocene 13 (4), 593–604.

Morhange, C., Hesnard, A., Marriner, N., 2011. La géoarchéologie littorale écartelée entre géo- et archéo-sciences ? Méditerranée 117, 55–60.

Moustaka, A., Skarlatidou, E., Tzannes, M.-C., & Ersoy, Y. (eds., 2004). Klazomenai, Teos and Abdera: metropoleis and colony. Proceedings of the International Symposium held at the Archaeological Museum of Abdera, Thessaloniki: University Studio Press.

Nerantzis, N., 2015. Pre-Industrial Iron Smelting and Silver Extraction in North-Eastern Greece: an Archaeometallurgical Approach. Archaeometry 58 (4), 624–641.

Orengo, H.A., Petrie, C.A., 2017. Large-scale, multi-temporal remote sensing of palaeo-river networks: A case study from Northwest India and its implications for the indus civilisation. Remote Sens. (Basel) 9, 1–20.

Orengo, H.A., Petrie, C.A., 2018. Multi-Scale Relief Model (MSRM): a new algorithm for the visualisation of subtle topographic change of variable size in digital elevation models. Earth Surf. Proc. Land. 43 (6), 1361–1369.

Papadopoulos, G., Diakogianni, G., Fokaefs, A., Ranguelov, B., 2011. Tsunami hazard in the Black Sea and the Azov Sea: A new tsunami catalogue. Nat. Haz. Earth Syst. Sci. 11, 945–963.

Papadopoulos, G., Fokaefs, A., 2005. Strong tsunamis in the mediterranean sea: A re-evaluation. ISET J. Earthq. Technol. 42, 159–170.

Papadopoulos, G., Gràcia, E., Urgeles, R., Sallares, V., De Martini, P.M., Pantosti, D., González, M., Yalciner, A.C., Mascle, J., Sakellariou, D., Salamon, A., Tinti, S., Karastathis, V., Fokaefs, A., Camerlenghi, A., Novikova, T., Papageorgiou, A., 2014. Historical and pre-historical tsunamis in the Mediterranean and its connected seas: Geological signatures, generation mechanisms and coastal impacts. Mar. Geol. 354, 81–109.

Pavlopoulos, K., Kapsimalis, V., Theodorakopoulou, K., Panagiotopoulos, I.P., 2012. Vertical displacement trends in the Aegean coastal zone (NE Mediterranean) during the Holocene assessed by geo-archaeological data. Holocene 22 (6), 717–728.

Perissoratis, C., Mitropoulos, D., 1989. Late Quaternary evolution of the northern Aegean shelf. Quat. Res. 32 (1), 36–50.

Peters, R., Jaffe, B., 2010. Identification of tsunami deposits in the geologic record; developing criteria using recent tsunami deposits. United States Geological Survey Open-File Report.

Pouzet, P., Maanan, M., 2020. Temporal approaches of historical extreme storm events based on sedimentological archives. J. Afr. Earth Sc. 162, 103710.

Psomiadis, D., Dotsika, E., Albanakis, K., Ghaleb, B., Hillaire-Marcel, C., 2018. Speleothem record of climatic changes in the northern Aegean region (Greece) from the Bronze Age to the collapse of the Roman Empire. Palaeogeogr. Palaeoclimatol. Palaeoecol. 489, 272–283.

Reimer, P.J., Austin, W.E.N., Bard, E., Bayliss, A., Blackwell, P.G., Bronk Ramsey, C., Butzin, M., Cheng, H., Edwards, R.L., Friedrich, M., Grootes, P.M., Guilderson, T.P., Hajdas, I., Heaton, T.J., Hogg, A.G., Hughen, K.A., Kromer, B., Manning, S.W., Muscheler, R., Palmer, J.G., Pearson, C., van der Plicht, J., Reimer, R.W., Richards, D.A., Scott, E.M., Southon, J.R., Turney, C.S.M., Wacker, L., Adolphi, F., Büntgen, U., Capano, M., Fahrni, S.M., Fogtmann-Schulz, A., Friedrich, R., Köhler, P., Kudsk, S., Miyake, F., Olsen, J., Reinig, F., Sakamoto, M., Sookdeo, A., Talamo, S., 2020. The IntCal20 Northern Hemisphere Radiocarbon Age Calibration Curve (0–55 cal. kBP). Radiocarbon 62 (4), 725–757.

Ruiz-Pérez, J.M., Carmona, P., 2019. Turia river delta and coastal barrier-lagoon of Valencia (Mediterranean coast of Spain): Geomorphological processes and global climate fluctuations since Iberian-Roman times. Quat. Sci. Rev. 219, 84–101.

Salomon, F., Goiran, J.P., Noirot, B., Pleuger, E., Bukowiecki, E., Mazzini, I., Carbonel, P., Gadhoum, A., Arnaud, P., Keay, S., Zampini, S., Kay, S., Raddi, M., Ghelli, A., Pellegrino, A., Morelli, C., Germoni, P., 2018. Geoarchaeology of the Roman port-city of Ostia: Fluvio-coastal mobility, urban development and resilience. Earth Sci. Rev. 177, 265–283.

Seeliger, M., Pint, A., Frenzel, P., Marriner, N., Spada, G., Vacchi, M., Başaran, S., Dan, A., Seeger, F., Seeger, K., Schmidts, T., Brückner, H., 2021. Mid- to late-Holocene sea-level evolution of the northeastern Aegean sea. Holocene 31 (10), 1621–1634.

Shanmugam, G., 2012. Process-sedimentological challenges in distinguishing paleo-tsunami deposits. Nat. Hazards 63 (1), 5–30.

Siani, G., Paterne, M., Arnold, M., Bard, E., Métivier, B., Tisnerat, N., Bassinot, F., 2000. Radiocarbon reservoir ages in the Mediterranean Sea and Black Sea. Radiocarbon 42 (2), 271–280.

Steffen, W., Broadgate, W., Deutsch, L., Gaffney, O., Ludwig, C., 2015. The trajectory of the anthropocene: The great acceleration. Anthropocene Review 2 (1), 81–98.

Stock, F., Knipping, M., Pint, A., Ladstätter, S., Delile, H., Heiss, A.G., Laermanns, H., Mitchell, P.D., Ployer, R., Steskal, M., Thanheiser, U., Urz, R., Wennrich, V., Brückner, A., 2016. Human impact on Holocene sediment dynamics in the Eastern Mediterranean - the example of the Roman harbour of Ephesus. Earth Surf. Proc. Land. 41 (7), 980–996.

Stournaras, G. (1984). Evolution et comportement d ' un système aquifère hétérogène : géologie et hydrogéologie du delta du Nestos (Grèce) et de ses bordures. Université Scientifique et Médicale de Grenoble.

Stuiver, M., Reimer, P.J., 1993. Extended 14C database and revised Calib 3.0 14C Age Calibration program. Radiocarbon 35 (1), 215–230.

Sylaios, G., Kamidis, N., Anastasiou, S., Tsihrintzis, V.A., 2013. Hydrodynamic response of Thassos Passage (N. Aegean Sea) to Nestos River discharge and meteorological forcing. Cont. Shelf Res. 59, 37–51.

Syrides, G., & Psilovikos, A. (2004). Geoarcheological investigations in the area of ancient Abdera. In A. Moustaka, E. Skarlatidou, M.-C. Tzannes, & Y. Ersoy (Eds.), Klazomenai, Teos and Abdera. Metropoleis and Colony. Proceedings of the International Symposium held at the Archaeological Museum of Abdera, Abdera, 2001 (pp. 351–359). Thessaloniki: 19th Ephorate of Prehistoric and Classical Antiquities of Komotini.

Vacchi, M., Rovere, A., Chatzipetros, A., Zouros, N., Firpo, M., 2014. An updated database of Holocene relative sea level changes in NE Aegean Sea. Quat. Int. 328–329, 301–310.

Vacchi, M., Marriner, N., Morhange, C., Spada, G., Fontana, A., Rovere, A., 2016. Multiproxy assessment of Holocene relative sea-level changes in the western Mediterranean: Sea-level variability and improvements in the definition of the isostatic signal. Earth Sci. Rev. 155, 172–197.

van der Geest, M., van Gils, J.A., van der Meer, J., Olff, H., Piersma, T., 2011. Suitability of calcein as an in situ growth marker in burrowing bivalves. J. Exp. Mar. Biol. Ecol. 399 (1), 1–7.

Votruba, G.F., Artzy, M., Erkanal, H., 2016. A set Archaic anchor arm exposed within P. oceanica matte at Klazomenai/Liman Tepe, Turkey: A contribution for understanding marine stratigraphy. J. Field Archaeol. 41 (6), 671–683.

Vött, A., Brückner, H., Schriever, A., Handl, M., Besonen, M., & Borg, K. Van Der. (2004). Holocene coastal evolution around the ancient seaport of Oiniadai, Acheloos alluvial plain, NW Greece. Coastline Reports, 1, 43–53.

Vött, A., Schriever, A., Handl, M., Brückner, H., 2007. Holocene palaeogeographies of the central Acheloos River delta (NW Greece) in the vicinity of the ancient seaport Oiniadai. Geodin. Acta 20 (4), 241–256.

Waters, C.N., Zalasiewicz, J., Summerhayes, C., Barnosky, A.D., Poirier, C., Gałuszka, A., Cearreta, A., Edgeworth, M., Ellis, E.C., Ellis, M., Jeandel, C., Leinfelder, R., McNeill, J.R., Richter, D.deB., Steffen, W., Syvitski, J., Vidas, D., Wagreich, M., Williams, M., Zhisheng, A.n., Grinevald, J., Odada, E., Oreskes, N., Wolfe, A.P., 2016. The Anthropocene is functionally and stratigraphically distinct from the Holocene. Science 351 (6269).

Xeidakis, G., Georgoulas, A., Kotsovinos, N., Delimani, P., Varaggouli, E., 2010. Environmental coastal degradation of the coastal zone of the West part of Nestos River Delta, N. Greece. Bulletin of the Geological Society of Greece 43, 1074–1084.

Xu, Q., Meng, L., Yuan, G., Teng, F., Xin, H., Sun, X., 2020. Transgressive wave- and tide-dominated barrier-lagoon system and sea-level rise since 8.2 ka recorded in sediments in northern Bohai Bay, China. Geomorphology 352, 106978.

Zalasiewicz, J., Waters, C.N., Summerhayes, C.P., Wolfe, A.P., Barnosky, A.D., Cearreta, A., Crutzen, P., Ellis, E., Fairchild, I.J., Gałuszka, A., Haff, P., Hajdas, I., Head, M.J., Ivar do Sul, J.A., Jeandel, C., Leinfelder, R., McNeill, J.R., Neal, C., Odada, E., Oreskes, N., Steffen, W., Syvitski, J., Vidas, D., Wagreich, M., Williams, M., 2017. The Working Group on the Anthropocene: Summary of evidence and interim recommendations. Anthropocene 19, 55–60.